UiT
THE ARCTIC UNIVERSITY OF NORWAY

Faculty of Health Sciences
Institute of Medical Biology

Optimisation of high-resolution fluorescence microscopy of normal- and preeclamptic placentas

—

Kristine Marie Bakken Knutsen

MBI-3911: Master's Thesis in Biomedicine, August 2019

Supervisors: Mona Nystad and Purusotam Basnet,
Women's Health and Perinatology Research Group, Department of Clinical Medicine

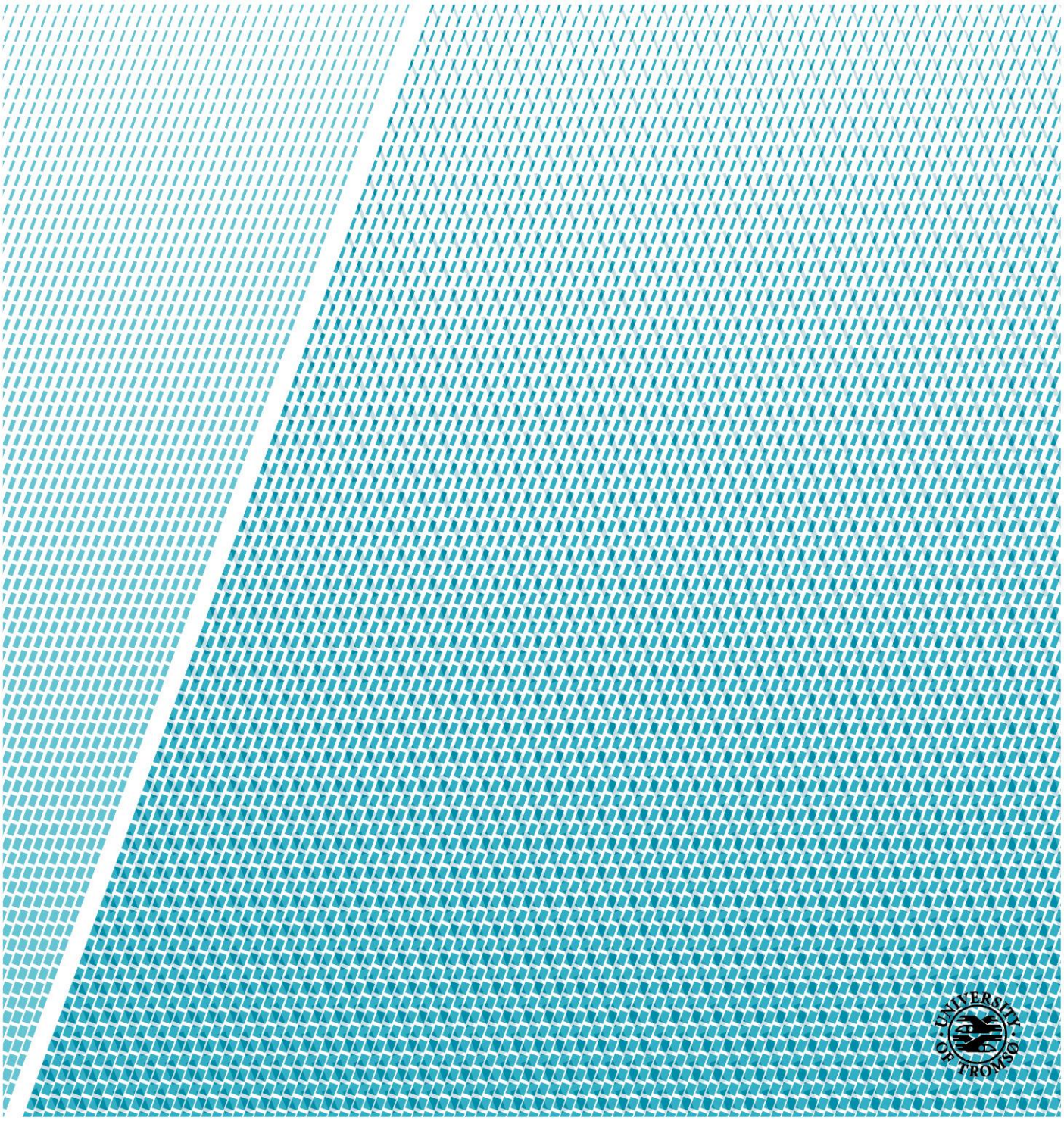

Acknowledgements

I am very grateful to everyone who have helped me during this interdisciplinary study, providing me with their expertise in the different parts.

A special thanks should be given to my main supervisor, Mona Nystad, PhD, for her exceptional guidance. She has included me in all phases; giving me the experience of the complexity of research. She has always given me help and support, advices, motivation and good conversations.

I would also like to thank my co-supervisor, Prof. Purusotam Basnet, for sharing his expertise and for his contributions to the thesis.

I wish to thank various people from the Optical Nanoscopy Research Group for their contributions to this study; Prof. Balpreet Singh Ahluwalia for allowing me to use their facilities; Deanna Wolfson for teaching me to use the microscopes and always being available for questions and help; and Luis Villegas for his useful tips, contributions and help with the imaging.

I would also like to thank Randi Olsen and Augusta Sundbø for always having an answer to my questions regarding collection and preservation of the material and supplying me with sections.

My gratitude also goes to the women who contributed material, the midwives and doctors at UNN, who made this study possible.

I am thankful to my friends and family: Sølvi for image editing and Mads his eyes for details. Last but not least, I am thankful to my mother and my boyfriend for their continuous support and encouragement.

Abbreviations

ABTS	3-ethylbenzothiazoline-6-sulphonic acid
Biomarkers	Biological markers
BMI	Body Mass Index
BSA	Bovine serum albumin
CMO	CellMask^{TM} orange
CT	Cytotrophoblast
DAPI	4',6-diamidino-2-phenylidole, dihydrochloride
DV	DeltaVision Elite High-resolution Microscope
EGTA	Ethylene glucol tetraacetic acid (ethylene glycol-bis (β-aminoethyl ether)-N,N,N',N'-tetraacetic acid)
ER	Endoplasmic reticulum
ET	Extravillous trophoblasts
EV	Extracellular vesicles
FA	Formaldehyde
FC	Fetal capillaries
FFPE	Formalin-fixed paraffin-embedded
Flt-1	Vascular endothelial growth factor receptor 1
hCG	Human chorionic gonadotropin
HELLP	Hemolysis elevated liver enzymes and low platelet count
HEPES	4-(2-hydroxyethyl)-1-piperazineethanesulfonic acid
IL	Interleukin
IUGR	Intrauterine growth restriction
MAP	Mean Arterial Pressure
MC	Maternal capillaries
MDA	Malondialdehyde
OD_{532}	Optical density at 530 nm wavelength
OD_{730}	Optical density at 730 nm wavelength
OMX	DeltaVision OMX V4 Blaze
PBS	Phosphate buffered saline

PE	Preeclampsia
PGF	Placental growth factor
PHEM	PPES-HEPES-EGTA-Magnesium sulphate
PIPES	1,4 piperazine bis (2-ethanosulfonic acid)
R^2	Regression coeffisient
REK Nord	Regional Committee for Medical and Health Research Ethics in Northern Norway
ROI	Region of interest
ROS	Reactive oxygen species
sFlt-1	Soluble fms-like tyrosine kinase 1
SIM	Structured illumination microscopy
SK	Syncytial knots
SRM	Super-resolution microscopy
ST	Syncytiotrophoblasts
TAC	Total antioxidant capacity
TBA	Thiobarbituric acid
TEM	Transmission electron microscope
TNF-α	Tumour necrosis factor alpha
UNN	University Hospital of Northern Norway
UPR	Unfolded protein response

Abstract

Preeclampsia (PE) affects 3-5 % of pregnant women and may lead to maternal and/or fetal death. The main theory of PE is placental ischemia, leading to a dysfunctional placenta and clinical signs as hypertension and proteinuria in the mother. The primary aim of the thesis was to implement and optimise a method for high-resolution microscopy of placental cryo-sections. Secondary aims were to compare the morphology, total antioxidant capacity (TAC) and the oxidative stress between normal- and preeclamptic placentas. Placental tissue from the fetal and maternal side were collected from three normal pregnant women and three preeclamptic women. For each patient; eight cryo-sections were prepared, four from each side of the placenta. Two were used as negative controls investigated for autofluorescence and two were used as positive controls labelled for morphological analysis. Positive controls were labelled with CellMask^{TM} Orange, staining cell membranes and 4',6-diamidino-2-phenylidole, dihydrochloride, staining nuclei. The TAC was determined by comparing the measured 3-ethylbenzothiazoline-6-sulphonic acid radical scavenging activity to an ascorbic acid standard curve. The oxidative stress was determined measuring the malondialdehyde content of the samples. Neither the normal nor the preeclamptic samples had autofluorescence affecting microscopy of the labelled sections. The method allowed visualisation of microscopic placental structures. In preeclamptic sections from the fetal side, there seemed to be more syncytial knots than in fetal sections from normal women. Bright red structures were detected in sections from the fetal side of preeclamptic samples and were not observed in normal sections. Because of their size, they were thought to be extravillous vesicles. The collection-, preservation- and labelling method was successfully implemented and is well suited for high-resolution microscopy. Although there were not found a significant difference in TAC and oxidative stress between normal- and preeclamptic placentas, neither on the fetal- or maternal side, the method is suited for placental tissue.

Table of contents

Introduction

Preeclampsia (PE), eclampsia and hemolysis, elevated liver enzymes and low platelet count (HELLP) syndrome are pregnancy-related hypertensive disorders, generally characterized by new-onset hypertension after 20 weeks of gestation (1). Pregnant women are diagnosed with PE when the blood pressure ≥140 mmHg systolic or ≥90 mmHg diastolic, in combination with proteinuria. Women affected with PE may also have placental dysfunction or dysfunction of maternal organs due to the increased blood pressure (2, 3). Eclampsia and HELLP syndrome are severe complications of PE. Eclampsia is characterized by new-onset grand mal seizures, whereas HELLP syndrome is characterized by hemolysis, elevated liver enzymes and low platelet count (4, 5).

Worldwide, PE affects 3-5 % of pregnant women (6). About 1 % of the cases are of a severe character, meaning that it is necessary to induce delivery preterm to avoid maternal death and/or stillbirth (7). PE affects women in both developed and developing countries and can occur in all pregnancies (6). Nulliparous women have a greater chance of being affected by PE compared to multiparous women, as the maternal immune system develops tolerance to paternal alloantigens following prolonged exposure. Men who have fathered a child where the pregnancy was complicated by PE has an increased risk of recurrence in later pregnancies. An extreme maternal age, either high or low, previous PE, obesity and chronic disease such as diabetes mellitus type I, renal disease and chronic hypertension, also increase the risk of being affected by PE. Due to the general increase in obesity, chronic disease and the increased age of nulliparous women, the incidence of PE is rising (8).

PE is divided into early-onset and late-onset, depending on whether the symptoms occur before or after week 34 (9). Generally, early-onset PE is more severe compared to late-onset PE. Regardless of type, PE is a significant risk factor for both maternal and fetal health, both during and after pregnancy. PE may have adverse effects such as acute pulmonary edema, epilepsy, kidney and liver dysfunction and intrauterine growth restriction (IUGR), in addition to other short-term complications during pregnancy (3, 9). Women who have been affected

by PE have an increased risk of being affected by cardiovascular diseases later in life (10). This also applies to the offspring from pregnancies complicated with PE.

For these reasons, blood pressure and urine are regularly checked and analysed throughout the pregnancy (11). Women diagnosed with PE are carefully monitored for the remaining duration of the pregnancy. Currently, there is no cure to the condition, and the treatment consists of controlling the hypertension and inducing delivery (12). Whether delivery is induced or not, depends on the gestational age and the maternal condition. In late-onset PE, the fetus is mature and delivery can safely be induced. In early-onset PE, the fetus is not fully mature and the health risk of the woman by continuing the pregnancy is weighed against the risk of premature birth.

Placental development and structure

During pregnancy, the fetus is contained in the amniotic sack in the uterus, surrounded by amniotic fluid (13). The placenta is the organ responsible for nutrient and oxygen transport from mother to fetus, including removal of carbon dioxide and other waste products. This transport is mediated through the umbilical cord, connecting the fetus to the placenta. Therefore, placental structure and function have a vital role in fetal development.

A normal mature human placenta is discoid shaped (Figure 1A and B), weighing about 500 g (14, 15). The placenta has a chorionic- and a basal plate, separated by the intervillous space (14). Towards the fetus is the chorionic plate with the umbilical cord, which connects the fetus to the placenta (Figure 1A). Towards the uterine wall is the basal plate with its cotyledons (Figure 1B). Cotyledons are small circular structures and the smallest functional unit of the placenta, consisting of a stem villus and the villi branching out from it (15). In total, a placenta has 15-28 cotyledons.

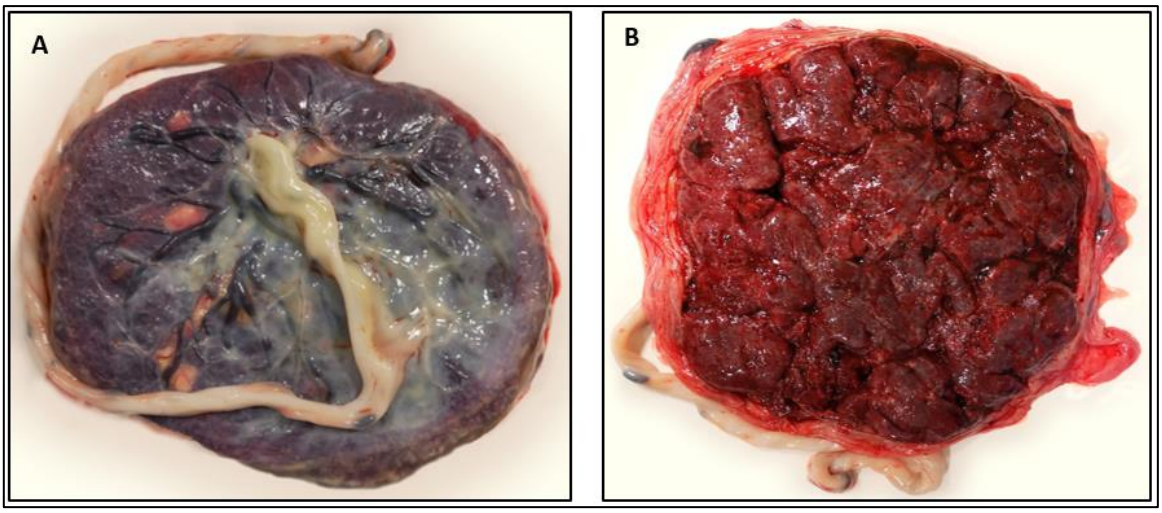

Figure 1: The macroscopic structure of a term human placenta. *A) Fetal side showing amnion and the umbilical cord. B) Maternal side with its membrane folded on the side to show the cotyledons.*

Placental development begins with the implantation of the blastocyst, which consists of two cell types; the outer trophoblasts and the inner cell mass (Figure 2A) (13). The trophoblasts develop into the placenta, whereas the inner cell mass develops into the fetus, and fetal membranes.

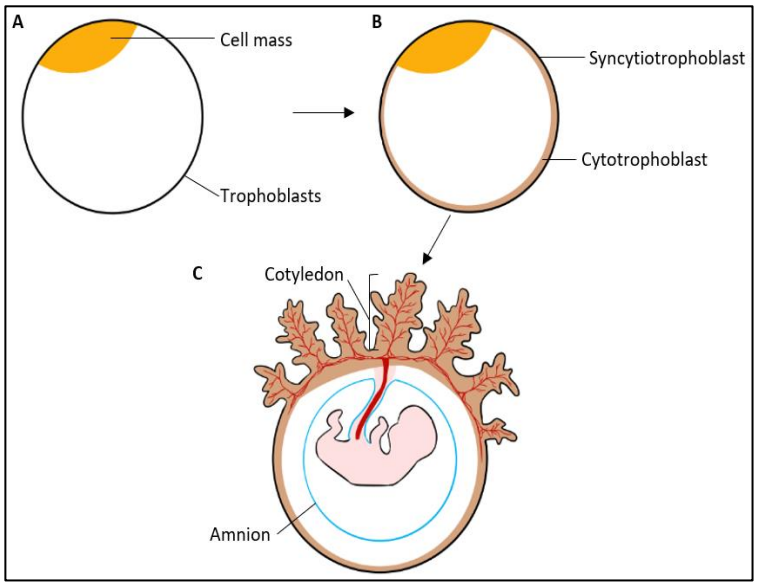

Figure 2: Schematic diagram illustrating the placental development. *A) Placental development starts when the blastocyst embeds into the endometrial epithelium. The blastocyst consists of two cell types; the outer trophoblasts and the inner cell mass. B) After implantation, the trophoblasts differentiate into two cell layers, the outer syncytiotrophoblasts and the inner cytotrophoblasts. C) The cytotrophoblasts proliferate and differentiate, thereby thickening the layer of syncytiotrophoblasts. Cytotrophoblasts secrete proteolytic enzymes, enabling syncytiotrophoblasts to send out projections towards the endometrium. Cytotrophoblasts and extraembryonic mesoderm follows the projections. The cotyledon is completed when the fetal capillaries are formed.*

Implantation starts with the blastocyst adhering to the endometrial epithelium in the uterus (13). Thereafter, the trophoblastic cells proliferate and differentiate into outer multinucleated syncytiotrophoblasts and inner cytotrophoblasts (Figure 2B). Cytotrophoblasts continue to proliferate and differentiate into syncytiotrophoblasts, thickening syncytiotrophoblastic layer. Spaces in the syncytiotrophoblastic layer called

lacunae are formed. When these fuse at a later stage in the development, the intervillous space is formed. Cytotrophoblasts secrete proteolytic enzymes, enabling syncytiotrophoblasts to send out projections, allowing the blastocyst to embed in the endometrium and form the early chorionic villi. When syncytiotrophoblasts erodes endometrial blood arteries, the lacunae are filled with blood. As separate lacunae merge, they form into the intervillous space.

Cytotrophoblasts and the extraembryonic mesoderm follows the syncytiotrophoblastic projections, continuing the development of the chorionic villi (13). At last, fetal blood vessels are formed, completing the villi (Figure 2C). Some fetal villi continues to grow towards the basal plate and decidua, anchoring it to the basal plate, whereas other fetal villi are free in the intervillous space. Figure 3 presents the placental structure when the placental development is completed.

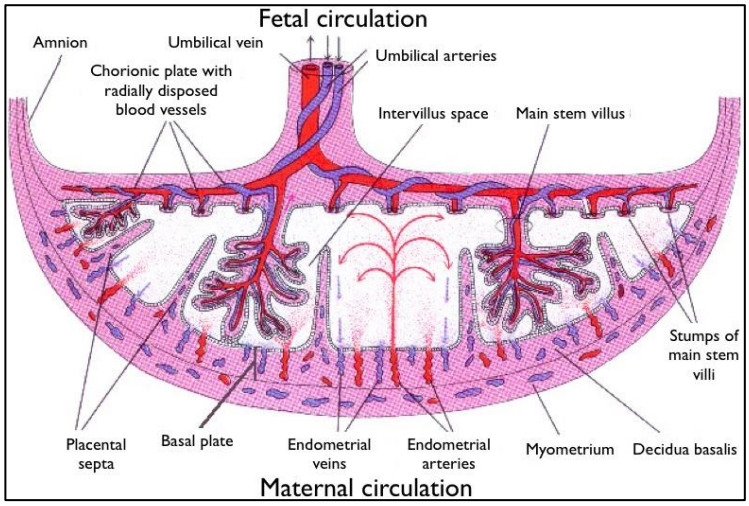

Figure 3: Placental structure. *The fetus is connected to the placenta through the umbilical cord. Towards the fetus is the chorionic plate containing fetal blood vessels. From the chorionic plate, cotyledons emerge into the intervillous space, separated by placental septa. Nutritious and oxygen rich maternal blood is lead into the intervillous space through endometrial arteries penetrating the basal plate, embedding the cotyledons in maternal blood. Nutritious depleted and carbon dioxide rich blood is lead out of the intervillous space through endometrial veins. The figure is retrieved and modified from: Moore and Persaud, 1993 (16).*

Endometrial arteries and veins penetrate the basal plate (17). Whereas the arteries supply the intervillous space with maternal blood, the veins remove maternal blood. Each stem villus is first divided into three to five intermediate villi, which is further branched into 10 to 12 terminal villi (18). The branching increases the surface of the cotyledon, making the nutritional exchange more effective. The insides of the cotyledons are of fetal origin, containing fetal capillaries.

As shown in Figure 4, a cotyledon is defined by three types of differentiated trophoblastic cells: syncytiotrophoblasts, cytotrophoblasts and extravillous trophoblasts (17).

Cytotrophoblasts define the inner lining, whereas syncytiotrophoblasts define the outer lining. Syncytiotrophoblasts are the only cells of fetal origin that are in contact with the maternal blood. The fetal capillaries in the core enable nutritional exchange between the maternal and fetal circulation by simple diffusion across the syncytium. In this way, the placenta also prevents mixing of fetal and maternal blood (19).

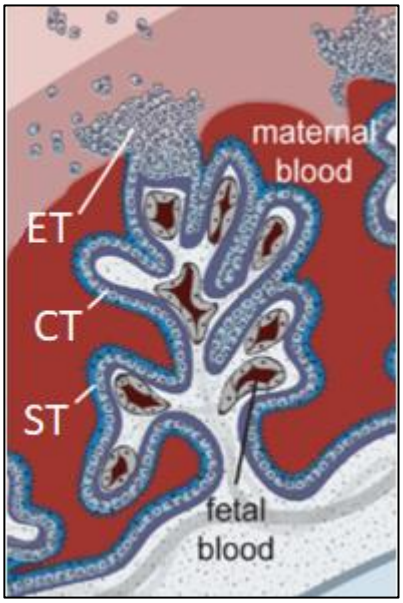

Figure 4: Overview of the cellular structure of a cotyledon illustrating the branched structure. *The villus is constituted of trophoblasts; an inner layer of cytotrophoblasts (CT) and an outer layer of syncytiotrophoblasts (ST). The core of the villus is fetal, containing fetal capillaries, which enable nutritional exchange between the maternal and fetal circulation by simple diffusion across the syncytium. The extravillous trophoblasts (ET) are differentiated invasive trophoblasts, that invade the walls of maternal endometrial arteries to increase their diameter. Grey matter inside the villi is mesenchymal core. The figure is retrieved and modified from: Zeldovich, et al., 2011 (17).*

During the second trimester, the fetal requirement of nutrients are increasing (20). In normal pregnancies, extravillous trophoblasts invade the walls of the maternal endometrial arteries to increase their diameter, thereby increasing the blood flow to the intervillous space (21).

The placenta in preeclampsia

The main theory of the etiology of PE is based on the placenta being ischemic (22, 23). This is supported by a study that found that the uteroplacental blood flow is reduced in women affected by PE (24). Placental ischemia is thought to occur when extravillous trophoblasts fail to increase the diameter of the maternal arteries, leading to a hypoxic placenta. During the ischemic period, the blood in the intervillous space has low levels of oxygen and nutrients (6). Decreased circulation leads to inflammation and oxidative stress. The placental hypoxia also leads to endoplasmic reticulum (ER) stress, release of proinflammatory cytokines and extracellular vesicles (EV) (Figure 5). When this occurs, the balance between anti-angiogenic and proangiogenic factors is skewed; anti-angiogenic factors increase while proangiogenic factors decrease. This leads to manifestation of clinical symptoms such as hypertension,

proteinuria, oedema, elevated liver enzymes and IUGR. Therefore, inflammation and oxidative stress affect the placental function, as well as fetal development and maternal health during pregnancy.

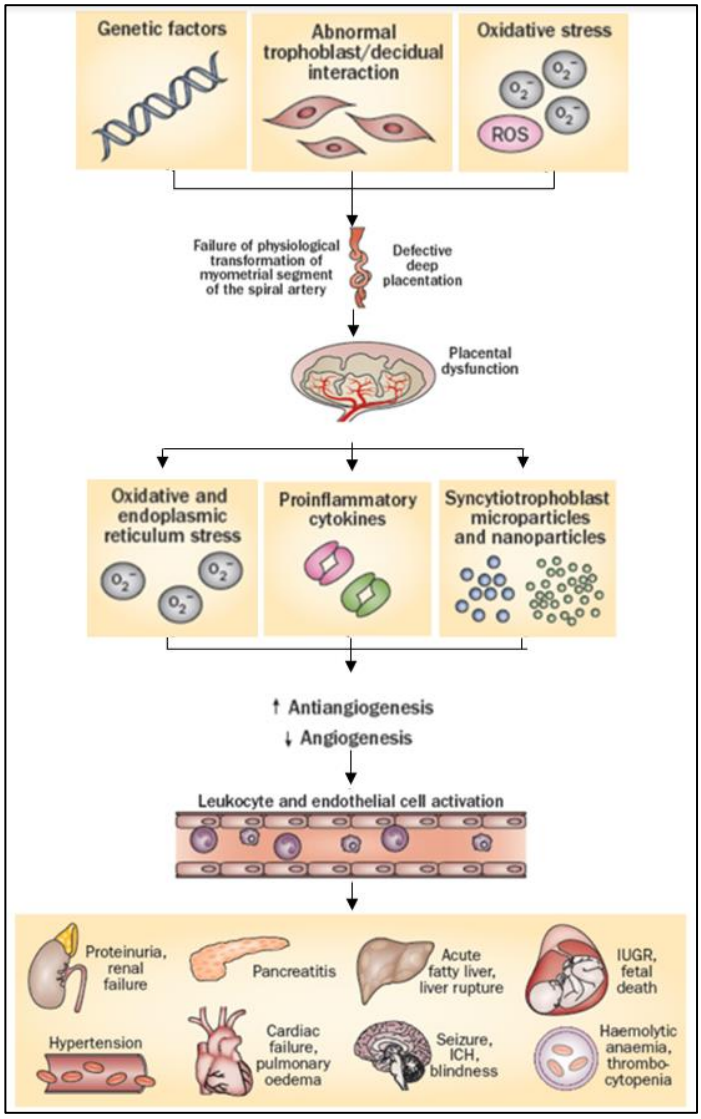

***Figure 5: Schematic illustration of the pathophysiology of preeclampsia (PE)**. Factors affecting the physiological transformation of the spiral arteries by the trophoblasts are genetic factors, abnormal trophoblast-decidua interaction and oxidative stress. When this occurs, the deep placentation is defective as the diameter of the spiral artery fail to increase. Less oxygen and nutrient rich blood enter the intervillous space, rendering the placenta as dysfunctional, causing endoplasmic reticulum- and oxidative stress. In addition, more proinflammatory cytokines are secreted into the maternal circulation by trophoblasts. Extracellular vesicles containing micro- and nanoparticles are also released into the maternal circulation. This leads to the secretion of more anti-angiogenic molecules and less proangiogenic molecules, activating endothelial cells, and thereby causing the clinical symptoms. The figure is retrieved and modified from: Chaiworapongsa et al., 2014 (6).*

Oxidative stress

Oxidative stress arises when the production of reactive oxygen species (ROS) exceeds the elimination, leading to ROS accumulating in the cell (25). ROS are highly reactive by-products of the oxygen metabolism in the cells, produced in different organelles with mitochondria being the largest contributor (26). As ROS have highly reactive properties, they can interact with central cellular structures, such as proteins, lipids and nucleic acids, thereby affecting their function (25).

Under normal conditions, there is a balance between the production and elimination of ROS. To maintain this balance, cells have different types of antioxidants and anti-oxidative systems to eliminate ROS, such as enzymes, peptides, vitamins and proteins (27). Some antioxidants are produced by the cells themselves, whereas other must be supplied through the diet. Reduced oxidative stress requires a balance between the amount of ROS and the total antioxidant capacity (TAC) of the cell or tissue.

Controlled levels of ROS are essential for normal cell function since ROS function as secondary messengers in several signalling pathways (28). These signalling pathways have different functions, such as activation of transcription factors, apoptosis and cell differentiation. Therefore, ROS should be generated, and the levels regulated for normal placental development and function (29).

Malondialdehyde (MDA) is a degraded lipid product and a well-studied biomarker of oxidative stress (30). As the levels of ROS increase, ROS react with surrounding cell membrane lipids to give lipid peroxidation products, such as MDA. Therefore, rising levels of MDA indicate increasing oxidative stress. By measuring the amount of MDA quantitatively, the oxidative stress level of the tissue can be determined. MDA reacts easily with thiobarbituric acid (TBA), resulting in a pink coloured adduct that can be measured quantitatively by spectrophotometry (27). MDA have been detected both in maternal circulation and placental tissue (30). It is shown that pregnant women in general have elevated levels of MDA. In normal pregnant women, the MDA level is balanced by increasing the TAC of the tissue, thereby eliminating ROS and preventing oxidative stress. Pregnant women affected by PE have higher levels of MDA compared to normal pregnant women. However, in women with PE, the TAC does not manage to overcome the increased production of ROS, leading to oxidative stress (31).

Long-term and chronic oxidative stress have been shown to contribute to the initiation of placental and endothelial dysfunction, in addition to induce inflammation by releasing proinflammatory cytokines (28, 32, 33). These mechanisms have a retroactive effect that increases the oxidative stress, creating a positive feedback loop.

Proinflammatory cytokines

Compared to normal pregnancies, pregnancies complicated with PE have higher levels of tumour necrosis factor (TNF)-α, interleukin (IL)-1β, IL-6 and IL-17, in addition to reduced levels of IL-4 and IL-10 (34-38). Among these cytokines, TNF-α, IL-1β, IL-6 and IL-17 are proinflammatory, whereas IL-4 and IL-10 are anti-inflammatory. The proinflammatory cytokines are present in the maternal circulation, increasing the endothelial permeability allowing proteins to leave the circulation and occur in the urine (39). TNF-α increases the vasoconstrictor endothelin-1 and reduces the vasodilator nitric oxide, leading to hypertension (37, 40).

Endoplasmic reticulum stress

The ER is an organelle consisting of several sacks called cisternae. This organelle is responsible for protein folding and transport and lipid synthesis. Placental hypoxia leads to an ischaemia-reperfusion injury in the intervillous space, which can lead to ER stress (41). During ER stress, proteins are incorrectly folded, resulting in accumulation of misfolded proteins in the ER. As a response to the ER stress, the unfolded protein response (UPR), a collection of signalling pathways are activated to overcome the ER stress. If the activation of UPR is not successful, the ER stress persists and leads to cessation of cell proliferation and apoptosis (42, 43). When trophoblasts undergo apoptosis, microparticles and nanoparticles are released into the maternal circulation (44).

Extracellular vesicles

EVs are lipid bilayers, ranging from 50 nm to 2 μm, containing cargo such as proteins, lipids and nucleic acids from the cell in which they were generated (45). There are two types of EVs classified by their size, content and origin: exosomes and microvesicles. Exosomes are 30 nm-150 nm in size and originate from the endolytic pathway, while microvesicles are 100 nm-1 μm in size and originate from direct budding or shedding, often in response to cellular stress (46).

EVs are thought to be a way of intercellular communication, where the cells in which the EV originated can interact with and change the activity of specific target cells (47). During pregnancy, placental cells, mainly the trophoblasts, release EVs to change the activity of maternal target cells, thereby altering the maternal physiology to accommodate fetal

requirements (47, 48). Such EVs have been found after six weeks of gestation (49). It has been proposed that EVs modulate central processes in pregnancy, such as cellular adaptations to pregnancy-related physiological changes, regulation of immune responses and migration and invasion of placental cells (47).

Compared to non-pregnant women, pregnant women have higher concentrations of EVs in the maternal circulation (50). Pregnant women affected with PE have an even higher concentration of EVs in the circulation and increases with disease severity.

Biological markers in pregnancy and preeclampsia

Biological markers (biomarkers) are measurable variables present in human tissues, cells or fluids that can be used either qualitative or quantitative to assess a person's physiological condition at a given time (51). There are four types of biomarkers; diagnostic, predictive, prognostic and therapeutic (52). Diagnostic biomarkers are used to diagnose a disease, predictive biomarkers are used to assess the response of a treatment, prognostic biomarkers are used to assess the progression of a condition with or without treatment, and therapeutic biomarkers are substances that can be used as targets for a therapy. As biomarkers have a variety of applications, biomarkers can be various substances found within the human body, such as cells, proteins, DNA and RNA (51).

In all pregnancies, cells and molecules originating from the placenta are shed and secreted into the maternal blood stream where they can be detected (53). These factors can either be passive, meaning they are a by-product of placental processes, or active, meaning they are released to change the maternal physiology to accommodate fetal requirements.

A biomarker used to confirm pregnancy is human chorionic gonadotropin (hCG), a hormone produced by the syncytiotrophoblastic cells in the placenta (54). The levels of hCG increase from implantation until week 10, where it peaks, before it drops slightly and stabilizes (54, 55). The hormone is present and detected in both the maternal circulation and urine. (55). As normal nonpregnant women do not produce hCG, the presence of the hormone in the maternal urine is a secure way of detecting pregnancy using simple commercial pregnancy tests.

Generally, both passive and active molecules are thought to be dysregulated during pregnancy-related diseases, making it possible to detect these molecules prior to the disease onset (53). All pregnancy-related diseases are thought to have several different potential biomarkers. In 2004, World Health Organization stated that «… there is no clinically useful screening test to predict the development of preeclampsia» (56). Since then, studies have found several potential biomarkers for PE, including soluble fms-like tyrosine kinase 1 (sFlt-1) and placental growth factor (PGF) (57, 58).

Fluorescent labelling methods and microscopy

Fluorescent microscopy is an important tool for examining tissue samples, utilising the ability of fluorescent molecules called fluorophores. Fluorophores absorb and emit light at specific wavelengths, thereby enabling visualisation of the labelled structures and molecules within cells and tissues (59).

Fluorophores absorb and emit light when their energy state is changed (60). When a photon hits a fluorophore, its electrons are excited to a higher energy level from its ground state level with lower energy. After a short time, the fluorophore transitions down to a lower energy level, releasing energy as vibrations and heat. Thereafter, the fluorophore transitions back to ground state level, releasing energy by emitting a photon. Following the principle of energy conservation, the incident photon is more energetic than the emitted photon. Each type of fluorophore has a characteristic excitation and emission spectra, making them ideal for observation in a microscope. Fluorescence microscopes can be used to detect fluorophores and can use different sources such as mercury lamps or lasers to illuminate the samples. The released photons are detected by a photodetector such as a camera. As each fluorophore emit light at a specific wavelength, different amounts of energy are required to excite them. By using different optical filters, it is possible to capture fluorescent light of specific wavelengths, making it possible to detect several fluorophores in one sample. Therefore, it is important to ensure that the fluorophore emits light of a wavelength that is detectable by the microscope that is used. By using fluorophores emitting different wavelengths of light, several structures can be visualised in the same section.

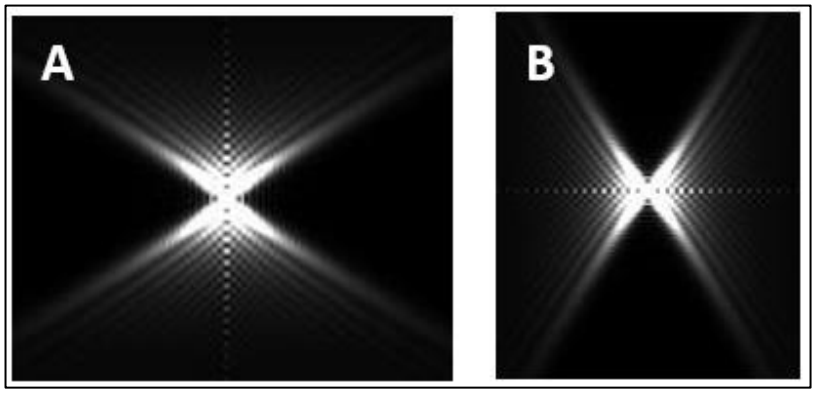

Figure 6: Point spread function in orthogonal view when there is an oil match. *A) How the light looks in the horizontal orientation. B) How the light looks in the vertical orientation. Villegas, 2018 (73).*

Deconvolution is a computational method used to improve images on fluorescent microscopes, enhancing the resolution by removing out of focus blur using algorithms (61). For this to be done, the point spread function must be optimised. Optimisation occurs when the refractive index of the immersion oil matches the cover glass and is controlled using orthogonal view on individual DV images. When symmetrical shapes are obtained (Figure 6), there is an oil match (62). There is an oil mismatch when asymmetrical shapes occur, and the immersion oil should be changed as oil mismatch can cause reconstruction artefacts.

Fluorescence microscopy has some disadvantages (60). Over time, fluorophores are photobleached, leading to a diminishing fluorescence. Structures within the cells may be autofluorescent, which may affect the imaging. Another limitation with conventional fluorescence microscopy, such as DV, is the resolution, which is limited by the diffraction of light to approximately 200 nm. Ultimately, this is what has led to the development of a new subset of fluorescence microscopy called super-resolution microscopy (SRM), allowing clear view of nanoscale subcellular structures.

A subsection within SRM is structured illumination microscopy (SIM), a method using a striped illumination pattern projected over the sample in a controlled fashion to improve the resolution (63). The Moiré fringes that result on the sample plane allow to visualise small details that otherwise would not be visible by the objective lens of the microscope. By changing the location of the illumination pattern, different parts of the sample become observable. Typically, nine images of an image field are taken to achieve a high-resolution image, each one with a specific phase and orientation. A specific algorithm is used to process the information, reconstructing an image of the biological sample with a resolution of

approximately 100 nm, increasing the resolution two-fold compared to DV. The PSF must also be checked in orthogonal view on individual SIM images to ensure oil matching.

Aims of the study

The primary aim of this thesis was to implement and optimise a collection and labelling method to better examine placental cryo-sections using high-resolution microscopy. The secondary objectives were to:

- Investigate morphological differences of the placenta from normal pregnant women and women affected with preeclampsia using high-resolution microscopy techniques for cryo-sections.
- Compare oxidative stress and total antioxidant capacity levels in placental tissue samples from normal pregnancies, and pregnancies complicated with preeclampsia using malondialdehyde assay and the ABTS scavenging activity of ascorbic acid, respectively.

Materials and methods

This study includes the collection, preparation and analysis of placental tissue samples from patients at the Department of Obstetrics and Gynaecology, University Hospital of Northern Norway (UNN). The study was approved by the Regional Committee for Medical and Health Research Ethics in Northern Norway (#2019/438) and Pasientvernombudet at UNN (reference number 2201). The research was performed following principles of the Helsinki declaration (64). All participants signed an informed consent form (Appendix A). The dignity of all participants was prioritized, and the study was observatory without inconvenience and discomfort for the participants. Collection of placental samples were performed after delivery and did not affect patient care. None of the research collaborators had any conflict of interest.

In this study, tissue from three normal- and three preeclamptic placentas were collected. Inclusion criteria for women with PE were new-onset, persistently elevated blood pressure (systolic blood pressure ≥140 mm Hg or a diastolic blood pressure ≥90mm Hg) and proteinuria after 20 weeks of gestation (65).

Clinical evaluation

The clinical evaluation was performed by the doctors at the Department of Obstetrics and Gynaecology, UNN, following the Norwegian guidelines for diagnosis and treatment of PE (65). Pregnant women suspected of being affected with or were diagnosed with PE were closely monitored and followed up.

Statistics of baseline information

Clinical data were analysed using IBM SPSS Statistics 21. Continuous variables are presented as mean ± standard deviation or median (range); categoric variables are presented as numbers (%). Differences between groups were tested using the Student's T-test for parametric data and with the Mann-Whitney U test or χ^2test for nonparametric and categorical variables. A *p*-value lower than 0.05 was considered as statistically significant.

Collection of placental tissue samples

Placental tissue samples from normal pregnant women and women affected with PE were collected from the Department of Obstetrics and Gynaecology at UNN. Chemicals used for sample collection are listed in Table 1.

Table 1: Chemicals used for collection of placental tissue samples.

Chemicals	Manufacturer	Reference	Purpose
Sodium chloride (9 mg/mL)	Fresenius Kabi AG	826968	Rinse the collected tissue of blood

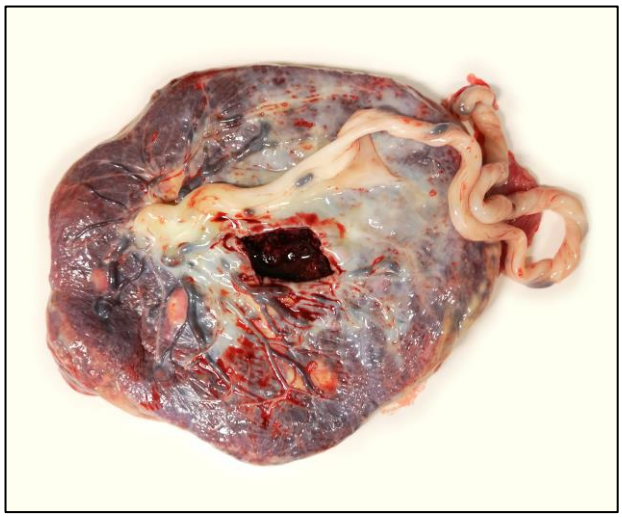

Figure 7: Image of a placenta showing where the tissue samples were obtained. *The image shows the fetal side with the umbilical cord. Tissue samples were taken approximately three cm from the umbilical cord.*

The placental samples were obtained within 30 min after delivery. All tissue samples were collected approximately three cm from the umbilical cord (Figure 7). Two tissue samples were collected for each study; one originating from the fetal side, and one originating from the maternal side.

The tissue samples were acquired by cutting through the placenta to obtain a piece containing both the maternal- and

fetal side (66). Thereafter, the piece was further cut to separate the maternal and fetal sides. The tissue pieces were rinsed for blood using 9 mg/mL sodium chloride and collected in separate tubes on ice for further preparation and storage.

Morphological study

Preparation of 4× PHEM buffer

PIPES-HEPES-EGTA-Magnesium sulphate (PHEM) is a no-toxic buffer used for immunocytochemical studies as it gives better ultrastructural preservation (67). It is often used for electron microscopy studies and was therefore used for temporarily preservation of the tissue pieces prior to fixation. Chemicals used for buffer preparation are listed in Table 2.

Table 2: Chemicals used to make the 4× PIPES-HEPES-EGTA-Magnesium sulphate (PHEM) buffer.

Chemicals	Manufacturer	Reference	Purpose
EGTA[1]	Sigma-Aldrich	E4378-100G	Used in PHEM
HEPES[2]	VWR Chemicals	441476L	Used in PHEM
PIPES[3]	Sigma	P6757-500G	Used in PHEM
Magnesium sulphate	Sigma-Aldrich	M7506-500G	Used in PHEM
5 M sodium hydroxide	Sigma-Aldrich	30620-1KG-R	Used in PHEM

[1] Ethylene glucol tetraacetic acid (ethylene glycol-bis (β-aminoethyl ether)-N,N,N',N'-tetraacetic acid) (EGTA)
[2] 4-(2-hydroxyethyl)-1-piperazineethanesulfonic acid (HEPES)
[3] 1,4 piperazine bis (2-ethanosulfonic acid) (PIPES)

First, 36.28 g of 1,4 piperazine bis (2-ethanosulfonic acid) (PIPES) were added to 225 mL ddH_2O and the pH was adjusted to 6.9 using 5 M sodium hydroxide. Then, 13 g of 4-(2-hydroxyethyl)-1-piperazineethanesulfonic acid (HEPES), 7.6 g of ethylene glucol tetraacetic acid (ethylene glycol-bis (β-aminoethyl ether)-N,N,N',N'-tetraacetic acid) (EGTA) and 1.98 g of magnesium sulphate were added and the volume was adjusted to 250 mL using ddH_2O. At last, the pH was adjusted to 6.9 using 5 M sodium hydroxide.

Storage of placental tissue samples

The collected tissue was fixed over night, immersed in gelatine and transferred to sucrose to prevent crystallisation during freezing. At last, the tissue was mounted on specimen carriers and frozen in liquid nitrogen. Equipment used for sample fixation and storage is listed in Table 3 and chemicals in Table 4.

Table 3: Equipment used to store collected placental tissue samples.

Equipment	Manufacturer	Reference	Purpose
VWR Digital Incubator	VWR	-	Liquify gelatine
Specimen carriers	Leica	167001950	Assembly of tissue pieces for storage
B7925 Tube Rotator	Agar Scientific	-	Ensure the tissue were immersed in gelatine and sucrose

Table 4: Chemicals used to store collected placental tissue samples.

Chemicals	Preparation	Manufacturer	Reference	Purpose
Fixative	15 mL 0.2 M PBS[1], 7.5 mL 8 % FA[2] diluted in 4× PHEM[3], 7.5 mL ddH_2O	-	-	Fixate tissue and preserve tissue morphology
FA (8 %)	7 mL 16 % FA in 7 mL 1x PHEM	-	-	Used in fixative
FA (16 %)	16 g FA in 100 mL ddH_2O	-	-	To further dilute to 8 % FA
FA	-	Sigma-Aldrich	158127-500G	Prepare 16 % FA
Gelatine (12 %)	12 g gelatine diluted in 100 mL ddH_2O	Fluka Analytical	48723-500G-F	Preserving tissue morphology; fill spaces and cavities in the tissue
PBS (0.2 M)	10 mL 1 M PBS in 40 mL ddH_2O	Oxoid LTD	BR0014G	Used in fixative
PBS (1 M)	1 g PBS in 1 L ddH_2O	Oxoid LTD	BR0014G	Washing
PHEM (1×)	10 mL 4× PHEM diluted in 30 mL ddH_2O	-	-	Prevent tissue degradation and dehydration of the tissue
PHEM (4×)	-	-	-	Dilute to 1× PHEM
Sucrose (2.3 M)	342 g sucrose diluted in 100 mL ddH_2O	Sigma-Aldrich	16104-1KG	Preventing crystallization during freezing

[1] Phosphate buffered saline (PBS)
[2] Formaldehyde
[3] PIPES-HEPES-EGTA-Magnesium sulphate buffer (PHEM)

The collected tissue samples were transferred to 5 mL of 1× PHEM. Thereafter, the tissue samples were cut in pieces of 1 mm^3, immersed in 5 mL of fixative and incubated at 4 °C over night.

After overnight incubation, the tissue samples were washed 2×5 min in 5 mL of 1 M phosphate buffered saline (PBS) followed by incubation in 1 mL 12 % gelatine in a tube rotator for 1 h at 37 °C. The tissue samples were then transferred to 1 mL of 2.3 M sucrose on ice and incubated in a tube rotator at 4 °C over night.

The tissue samples were assembled on specimen carriers before being frozen in liquid nitrogen. The specimen carrier was applied 2.3 M sucrose before a tissue sample was transferred onto it and frozen in liquid nitrogen. For each patient, five specimen carriers were prepared from each side of the placenta. The unassembled tissue samples were preserved in 2.3 M sucrose and frozen in liquid nitrogen with the assembled tissue samples.

Poly-L-lysine coating of cover glasses

To make cells adhere to the cover glass and avoid detachment during labelling and washing, cover glass was coated with poly-L-lysine. Equipment used to coat cover glass is listed in Table 5 and chemicals in Table 6.

Table 5: Equipment used to coat cover glasses with poly-L-lysine.

Equipment	Manufacturer	Reference	Purpose
13 mm #1.5 Cover glass	VWR	631-0150	-

Table 6: Chemicals used to coat cover glasses with poly-L-lysine.

Chemicals	Preparation	Manufacturer	Reference	Purpose
Poly-L-lysine (0.2 mg/mL)	0.2 mg poly-L-lysine in 1 mL ddH_2O	Sigma	P1274	Provide adherence between tissue section and cover glass

Cover glasses were cleaned using ethanol, rinsed with ddH_2O and air dried on filter paper. Thereafter, 30-50 µL of 0.2 mg/mL poly-L-lysine were pipetted in the centre of the cover glass and settled for 30 min in a moist chamber. The cover glasses were rinsed with ddH_2O and

dried on filter paper over night at room temperature. Poly-L-lysine coated cover glasses were stored in dust-free dishes at room temperature until use.

Labelling of cryo-sections

Ultrathin cryo-sections were prepared using the Tokuyasu method (68). The Tokuyasu method is a gentle method solidifying the tissue by freezing and cutting cryo-sections. From each placental sample, eight cryo-sections were prepared; four from the fetal side of the placenta and four from the maternal side of the placenta. From each side, two cryo-sections were prepared as negative controls for investigation of autofluorescence, and two cryo-sections were stained with CellMask^{TM} Orange (CMO) and 4',6-diamidino-2-phenylidole, dihydrochloride (DAPI) to visualize cellular structures. Equipment used for labelling is listed in Table 7 and chemicals in Table 8.

Table 7: Equipment used to label the placental cryo-sections.

Equipment	Manufacturer	Reference	Purpose
British Standard Microscope slides	ThermoFisher	10144633CF	Assemble cover glass
Nail polish	-	-	Seal the edge of the mounted cover glass
Poly-L-lysine coated cover glass with tissue sections	-	-	-
Six-edged nut	-	-	Ensure the cover glass was in level

Table 8: Chemicals used to label the placental cryo-sections.

Chemicals	Preparation	Manufacturer	Reference	Purpose
BSA[1] (1 %)	0.5 g BSA in 50 mL 1 M PBS[2]	Sigma	A8022	Blocking
CMO[3] (250 ng)	0.5 µL CMO in 999.5 µL 1 M PBS	ThermoFisher	C10045	Staining cell membranes
DAPI[4] (5 ng)	1 µL DAPI in 999 µL 1 M PBS	Life technologies	S33025	Staining cell nuclei
Methyl cellulose (1 %)	250 µL 2% methyl cellulose in 250 µL 2.3 M sucrose	-	-	Prevent the section from drying out
Methyl cellulose (2 %)	2 g methyl cellulose in 100 mL ddH_2O	Sigma	M6385-100G	To further dilute to 1 % methyl cellulose
PBS (1 M)	1 g PBS in 1 L ddH_2O	Oxoid LTD	BR0014G	Washing and dilution of CMO and DAPI
Prolong Gold	-	Invitrogen	P36934	Mounting medium
Sucrose (2.3 M)	342 g sucrose diluted in 100 mL ddH_2O	Sigma-Aldrich	16104-1KG	Prepare methyl cellulose (1 %)

[1] Bovine serum albumin (BSA)
[2] Phosphate buffered saline (PBS)
[3] CellMask™ Orange (CMO)
[4] 4',6-diamidino-2-phenylidole, dihydrochloride (DAPI)

For each patient sample, eight ultrathin cryo-sections (1 µm) were prepared using the Tokuyasu method. Four sections originated from the fetal side of the placenta and four sections originated from the maternal side of the placenta. The sections were prepared on separate poly-L-lysine-coated cover glasses and covered with 1 % methyl cellulose. Sectioning was performed by engineer at the Facility for Advanced Microscopy, UiT – The Arctic University of Norway.

All sections were cooled on a parafilm covered metal plate on ice for 10 min and washed 3×7 min with 100 µL of 1 M PBS. Between each wash, the sections were prevented from drying by adding new PBS immediately after removing the previous wash, using absorbent paper. Following washing, the metal plate with the sections were taken off the ice, placed on bech and blocked in 100 µL of 1 % bovine serum albumin (BSA) for 30 min. Thereafter, the sections were washed 2×5 min in 100 µL of 1 M PBS.

From each side of the placenta, two sections were labelled. To label the sections, 100 µL of CMO (250 ng) were added, and the sections were incubated for 10 min protected from light. The sections were then washed 2×5 min in 100 µL of 1 M PBS as previously described. Thereafter, 100 µL of DAPI (5 ng) were added and the sections were incubated in the dark for 5 min. At last, the sections were washed 3×5 min in 100 µL of MilliQ-water and mounted.

The remaining two sections were prepared as unlabelled negative controls. These were washed 3×5 min with 100 µL of ddH_2O and mounted as described for the labelled sections.

Mounting was performed by adding one small drop of Prolong Gold in the centre of a glass slide. The cover glass was immediately placed on top with the tissue section facing the mounting medium. If air bubbles appeared, the cover glass was carefully tapped with a plastic tweezer. A six-edged nut was placed on top of the cover glass to ensure that it was level. Thereafter, the sample was incubated for 1 h protected from light before the edge of the cover glass was sealed using nail polish. The mounted sections were stored at 4 °C, protected from light.

Microscopy

The unlabelled negative controls were only inspected for autofluorescence using the DeltaVision Elite High-resolution Microscope (DV), whereas the labelled slides were imaged using both the DV and the DeltaVision OMX V4 Blaze (OMX) microscopes. SoftWoRx and Fiji were used to reconstruct and process the images, respectively. Equipment used for microscopy is listed in Table 9 and chemicals in Table 10.

Table 9: Equipment used for microscopy of the prepared tissue sections.

Equipment	Manufacturer	Reference	Purpose
DeltaVision Elite High-resolution Microscope (DV)	GE Healthcare	-	Localize the sample and ROI[1]
DeltaVision OMX V4 Blaze (OMX)	GE Healthcare	-	Examine ROI
SoftWoRx	GE Healthcare	-	Image reconstruction
Fiji	Fiji Contributors	-	Image processing

[1] Region of interest (ROI)

Table 10: Chemicals used for microscopy of the prepared tissue sections.

Chemicals	Manufacturer	Reference	Purpose
Cargille Laser Liquid Code 5610 (1.514)	GE Healthcare	20130	Optimize the PSF[1] on the OMX[2]
Cargille Laser Liquid Code 5610 (1.516)	GE Healthcare	20130	Optimize the PSF on the OMX
Cargille Laser Liquid Code 5610 (1.518)	GE Healthcare	20130	Optimize the PSF on the OMX
Ethanol (100 %)	-	-	Clean the microscope slides

[1] Point spread function (PSF)
[2] DeltaVision OMX V4 Blaze (OMX)

Prior to microscopy, the slide was cleaned using hand soap and water, carefully dried and cleaned with 100 % ethanol. The unlabelled sections were only checked for autofluorescence using the DV microscope at 10× magnification. The labelled sections were localized using the DV microscope at 10× magnification, gradually increasing the magnification to 20× magnification to find regions of interest (ROI). Coordinates of the ROIs were used to find the same regions on the OMX to further investigate them at 60× magnification with immersion oil. To ensure that the refractive index of the oil matched the cover glass, the PSF of single emitters was observed in orthogonal view. If symmetrical shapes were not obtained, the oil was changed accordingly.

During microscopy, the images were reconstructed using SoftWoRx. After microscopy, the images were processed using Fiji.

Oxidative stress study

The tissue samples were collected at different times and were stored at -70 °C until measurement. On the day of analysis, the samples were thawed, partly dried with tissue paper, weighed and homogenised by sonication. Equipment used for tissue homogenisation is listed in Table 11 and Table 12.

Table 11: Equipment used to homogenise the placental samples.

Equipment	Manufacturer	Reference	Purpose
Beckman Microfuge 11	Beckman	-	Spin down cell debris
Branson Sonifier 250	Branson Ultrasonic	-	Homogenize the tissue

Table 12: Chemicals used to homogenise the placental samples.

Chemicals	Preparation	Manufacturer	Reference	Purpose
PBS[1] Dulbecco (0.1 M)	10 mL 1 M PBS Dulbecco in 100 mL ddH_2O	Sigma-Aldrich	D8537-500ML	Homogenize the tissue

[1] Phosphate buffered saline (PBS)

After being transferred to ice, the samples were frozen at -70 °C for long-time storage. When enough samples were collected, the oxidative stress and TAC of all samples were measured simultaneously to ensure equal conditions.

The frozen placental samples were thawed for an hour at room temperature. The samples were partly dried with tissue paper and 0.2-0.4 g sample were weighed and transferred to separate tubes. Each sample was added 0.1 M PBS Dulbecco with the ratio of 0.5 mL/100 mg sample. All samples were sonicated separately with a probe sonicator (30 cycles/30 sec) and centrifuged at 1500×*g* for 20 min at 4 °C. From each sample, 2 mL supernatant was transferred to new tubes and kept at 4 °C over night.

Total antioxidant capacity assay

The TAC of the placental samples was measured using 2,2'-azino-bis(3-ethylbenzothiazoline-6-sulphonic acid) (ABTS) radical scavenging activity by the antioxidant molecules in the tissue sample (69). To determine the antioxidant content in the tissue samples, the optical density at 730 nm wavelength (OD_{730}) of each tissue sample after the reaction with ABTS radicals was compared to a standard curve generated using ascorbic acid (a vitamin C equivalent). The intensity of the green colour of the ABTS radicals decreases as the amount of ABTS radicals is reduced, showing the TAC in the samples. Raw data is presented in Appendix B. Equipment used for TAC measurement is listed in Table 13 and chemicals in Table 14.

Table 13: Equipment used to measure the total antioxidant capacity (TAC) of the placental samples.

Equipment	Manufacturer	Reference	Purpose
Agilent 8453 UV-Visible spectrophotometer	Agilent Technologies	-	Measure OD_{730}
Beckman Microfuge 11	Beckman	-	Centrifuge
Semi-Micro Cells	Agilent Technologies	-	Cuvette used to measure optical density (OD_{730}[1])
UV visible system (software)	Agilent Technologies	-	Visualize the measurement

[1] Optical density at 730 nm wavelength (OD)

Table 14: Chemicals used to measure the total antioxidant capacity (TAC) of the placental samples.

Chemicals	Preparation	Manufacturer	Reference	Purpose
ABTS[1] (7.4 µM)	4.06 mg ABTS in 1000 µL ddH_2O	Sigma-Aldrich	A1888-1G	Generate ABTS radicals
Ascorbic acid (1 mg/mL)	100 µL 100 mg/mL ascorbic acid in 900 µL ddH_2O	-	-	To further dilute to 100 µg/mL ascorbic acid
Ascorbic acid (100 mg/mL)	9.2 mg ascorbic acid in 920 µL water	Sigma-Aldrich	A2218-25G	To further dilute to 1 mg/mL ascorbic acid
Ascorbic acid (100 µg/mL)	200 µL 1 mg/mL ascorbic acid in 900 µL ddH_2O	-	-	Make standard solution for the standard curve
Potassium peroxodisulfate (2.6 µM)	0.70 mg potassium peroxodisulfate in 1 mL ddH_2O	Merck	105092	Generate ABTS radicals

[1] 2,2'-azino-bis(3-ethylbenzothiazoline-6-sulphonic acid) (ABTS)

ABTS radicals were generated by mixing 3 mL 7.4 µM ABTS with 3 mL 2.6 µM potassium peroxodisulfate, followed by a 24 h incubation protected from light at room temperature to obtain dark green ABTS radicals. The green ABTS radicals were diluted with 200 mL ddH_2O to achieve an approximate OD_{730} of 0.7 for the ABTS radicals measuring with a UV spectrophotometer. To set reference on the UV spectrophotometer at OD_{730}, 600 µL ddH_2O was used. All measurements were made using a 700 µL cuvette.

Ascorbic acid was prepared as a stock solution of 10 mg/mL and diluted 100 times to prepare a standard solution of 100 µg/mL, as shown in Table 14. From the standard solution, 140, 120, 100, 80, 60, 40, 20, 10 and 0 µL were diluted to 1 mL with ddH_2O to make the following standard concentrations: 14, 12, 10, 8, 6, 4, 2, 1 and 0 µg/mL, respectively. For each standard concentration, three independent measurements were taken. From each standard concentration, 300 µL was mixed with 300 µL ABTS radicals and incubated for 30 min at room temperature. After incubation, OD_{730} of each sample was measured with the UV spectrophotometer.

When the measurements of the standard curve were completed, 1 mL tissue lysate was transferred to a new tube and centrifuged at 10 000×*g* for 20 min. Three independent measurements for each placental sample were taken. To measure TAC for the tissue samples, 10 µL suspension (equivalent to 1 mg tissue), 290 µL ddH_2O, and 300 µL ABTS radicals were mixed and incubated for 30 min. After the incubation, the OD_{730} of each sample was measured with a UV spectrophotometer. The TAC of the samples was determined by comparing the OD_{730} of each sample to the ascorbic acid standard curve.

Oxidative stress assay

The oxidative stress in the placental tissue samples were determined by measuring their MDA content. This was performed using the Lipid Peroxidation (MDA) Assay kit, with some adjustments from the manufacturer's protocol to adapt it to placental samples (70). To determine the MDA content in the tissue samples, the optical density at 532 nm wavelength (OD_{532}) of each sample was compared to a standard curve generated using MDA. As the intensity of the pink colour increases, the concentration of MDA increases, showing the oxidative stress in the samples. Raw data is presented in Appendix C. Equipment used for MDA measurements is listed in Table 15, kits in Table 16 and chemicals in Table 17.

Table 15: Equipment used to measure the oxidative stress in the placental samples.

Equipment	Manufacturer	Reference	Purpose
Falcon 96-well plate	Corning	303572	Measure MDA concentration in standard- and tissue samples
Epoch Microplate Spectrophotometer	BioTek Instrument	-	Measure the optical density of each well

Table 16: Kit used to measure the oxidative stress in the placental samples.

Kit	Manufacturer	Reference	Component	Preparation	Purpose
Lipid Peroxidation (MDA[1]) Assay kit	Sigma-Aldrich	MAK085-1KT	MDA lysis buffer	-	Lysate cells
			MDA standard (0.1 M)	10 µL 4.17 M MDA in 407 µL ddH_2O	To further dilute to 2 nM MDA
			TBA[2]	-	Create pink adduct

[1] Malondialdehyde (MDA)
[2] Thiobarbituric acid (TBA)

Table 17: Chemicals used to measure the oxidative stress in the placental samples.

Chemicals	Preparation	Manufacturer	Reference	Purpose
MDA[1] standard (2 mM)	20 µL 0.1 MDA in 980 µL ddH_2O	Sigma-Aldrich	-	Make the standard curve

[1] Malondialdehyde (MDA)

MDA was prepared as a stock solution of 0.1 M, which was diluted to 2 mM as shown in Table 17. Various concentrations of MDA were used to make the standard curve; 10, 8, 6, 4, 2 and 0 µL of 2 mM MDA was diluted to 200 µL with ddH_2O to make the following standard concentrations of 20, 16, 12, 8, 4 and 0 nM, respectively. From each standard concentration of MDA, 200 µL was mixed with 600 µL thiobarbituric acid (TBA). To measure the MDA content in the samples, 100 µL (equivalent to 10 mg tissue) of supernatant of each tissue sample was mixed with 100 µL lysis buffer and 600 µL TBA. Both the standard and the tissue samples were heated in a water bath at 90 °C for 1 h and cooled down on ice for 10 min to obtain a light pink-coloured MDA-TBA adduct.

From the reaction mixture, 200 µL of each standard and tissue sample were transferred to two separate wells on a 96-well plate with the layout shown in Figure 8. OD_{532} for each MDA

standard and tissue sample were measured spectrophotometrically by an enzyme-linked immunosorbent assay plate reader.

	1	2	3	4	5	6	7	8	9	10	11	12
A												
B		0 nM	0 nM	4 nM	4 nM	8 nM	8 nM	12 nM	12 nM	16 nM	16 nM	
C		20 nM	20 nM									
D		1P-F	1P-F	1P-M	1P-M	2P-F	2P-F	2P-M	2P-M	3P-F	3P-F	
E		3P-M	3P-M									
F		1N-F	1N-F	1N-M	1N-M	2N-F	2N-F	2N-M	2N-M	3N-F	3N-F	
G		3N-M	3N-M									
H												

Figure 8: Schematic diagram showing the layout on the 96-well plate. *To each well, 200 µL of solution were added. Rows B and C contain the different concentrations of the MDA standard, whereas rows D, E, F and G contain the tissue samples. "N" denotes samples from a normal placenta, whereas "P" denotes samples from a preeclamptic placenta. "F" denotes samples from the fetal side, whereas "M" denotes samples from the maternal side.*

Statistics

The mean OD_{730} and OD_{532} were calculated for the TAC and MDA assays, respectively. The mean OD for each of the assays was used to calculate the mean antioxidant concentration (µg ascorbic acid/mg placental tissue) and the mean MDA concentration (nM MDA). To evaluate the statistical significance of the normal- and preeclamptic samples, Student's T-test was used, and the *p*-values were determined. A *p*-value lower than 0.05 was considered as significant.

Results

Phenotype of the study population

The baseline demographic and clinical characteristics of the study population were routinely collected by midwifes and doctors at the Department of Obstetrics and Gynaecology, UNN, and is presented in Table 18. The mean proteinuria level in patients with PE was median

2 g/L (ranging from 1 to 3 g/L). None of the women included in the study had HELLP syndrome. In the preeclamptic group, two women delivered by caesarean section because of an acute deterioration of the patient's condition. One woman in the normal group also had caesarean delivery. None of the women who delivered by caesarean section were in labour. The two other women in the normal group had vaginal delivery and one in the PE group. In each group, one woman had her labour induced.

Table 18: Selected clinical parameters of the preeclamptic and normal group. *The differences were tested using Student's T-test for parametric variables and with the Mann-Whitney U test or χ^2test for nonparametric and categorical variables, as appropriate. N/A, not applicable.*

	Preeclampsia (n=3)	**Normal (n=3)**	***p*-value**
Maternal age[a]	35±2.19	33±0	0.488
BMI[1] before delivery[a]	23.8±3.50	25.1±1.46	0.752
Primipara n (%)	2 (66.67)	2 (66.67)	1
Urine Stix protein (g/L)[b]	2 (1-3)	N/A	-
MAP[2]	117.78±3.37	91.56±5.32	0.014
Middle cerebral artery pulsatility index[a]	1.32±0.24	1.39±0.02	0.842
Umbilical artery pulsatility index[a]	1.22±0.45	0.90±0.00	0.620
Gestational age at delivery (weeks)[a]	34±3.71	40±0.67	0.230
Caesarean section n (%)	2 (66.67)	1 (33.3)	0.000
Neonatal birth weight (g)[a]	2812±965	3512±131	0.512
Placental weight (g)[a]	484±107	578±14	0.432
5 min APGAR score (median range)[b]	10 (9-10)	10 (10-10)	0.667
Arterial cord blood pH[a]	7.26±0.04	7.23±0.07	0.825
Arterial cord blood Base Excess[a] (mmol/L)	-2.80±1.72	-10.15±0.65	0.048
Venous cord blood pH[a]	7.28±0.03	7.28±0.07	0.983
Venous cord blood Base Excess[a] (mmol/L)	-3.70±2.17	-10.60±0.90	0.097

[1] Body mass index (BMI)
[2] Mean arterial pressure (MAP)
[a] Data are given as mean ± standard deviation
[b] Data given as median (range)

One of the women in the PE group had early-onset PE (gestational week 27+3) and was admitted over time due to complications of her PE. The baby was premature and was admitted to the intensive care unit after delivery. The patient record stated IUGR during pregnancy and was found on repeated ultrasound scanning.

Morphological study

In total, eight sections were prepared from three normal- and three preeclamptic placental tissue samples, four from each side of the placenta. From these, two sections were prepared

as negative controls, whereas the other two sections were labelled with a membrane specific marker, CMO, and a nucleic acid specific marker, DAPI. Autofluorescence was detected by using the DV microscope. ROIs on the labelled sections were detected by using the DV microscope, which where further investigated using the OMX microscope.

Autofluorescence of placental cryo-sections

The autofluorescence of a normal placenta is presented in Figure 9 at 10× magnification. Figure 9A shows the autofluorescence of the fetal side, whereas Figure 9B shows the autofluorescence of the maternal side.

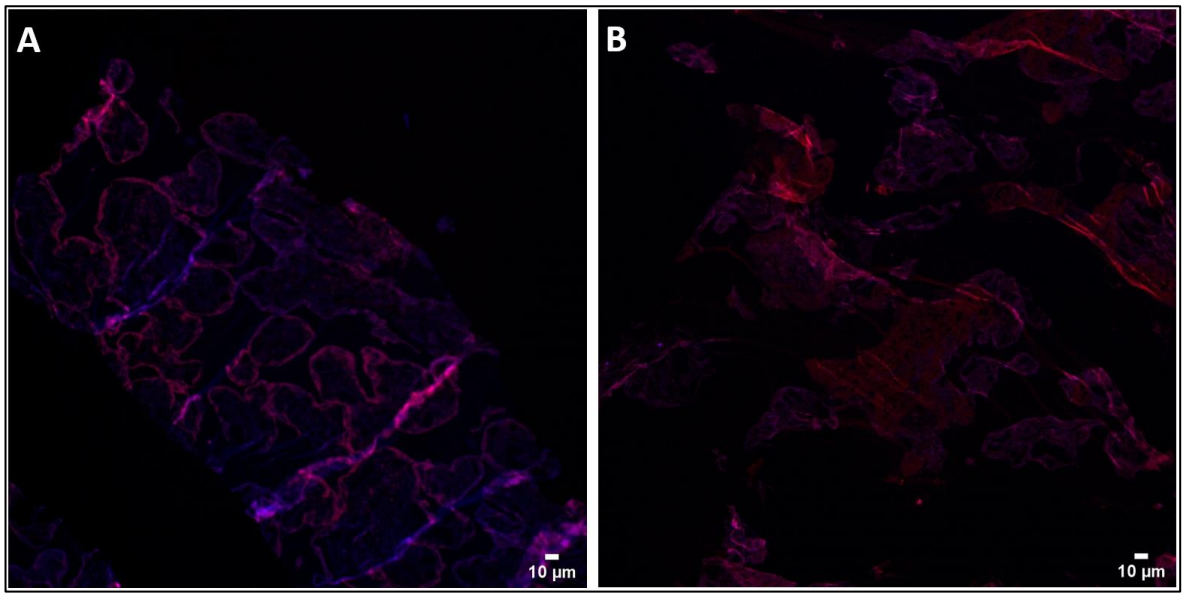

Figure 9: Overview images at 10× magnification of unstained cryo-sections of a normal placenta, showing the autofluorescence. *A) The fetal side of the normal placenta. B) The maternal side of a normal placenta.*

Figure 10 shows the autofluorescence of a preeclamptic placenta at 10× magnification; Figure 10A shows the autofluorescence of the fetal side, whereas Figure 10B shows the autofluorescence of the maternal side.

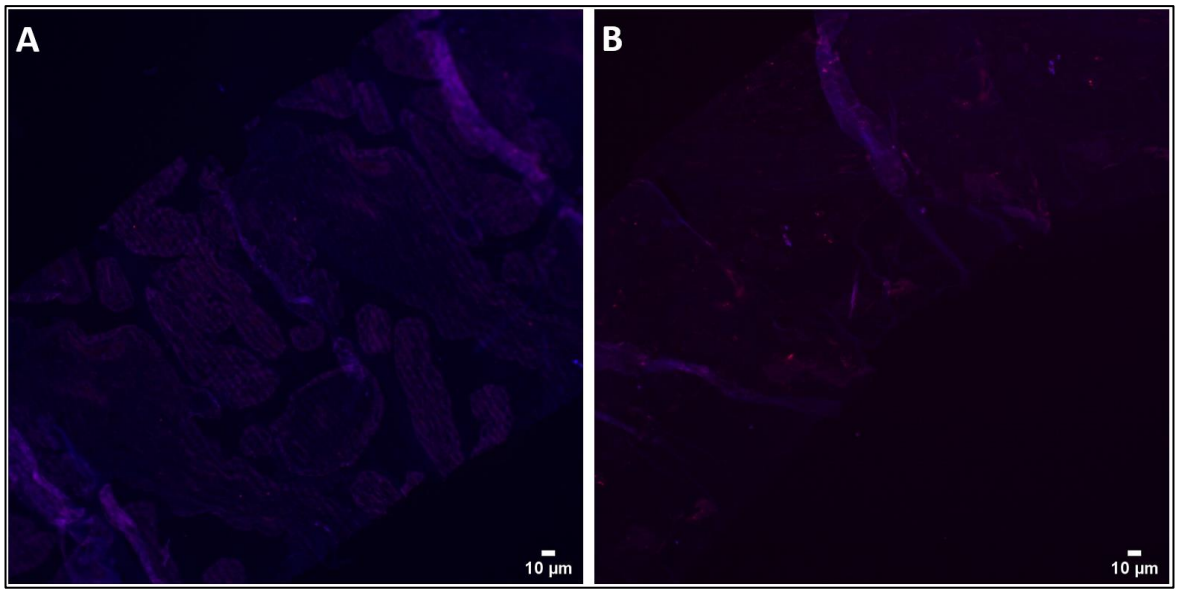

Figure 10: Overview images at 10× magnification of unstained cryo-sections of a preeclamptic placenta, showing the autofluorescence. *A) The fetal side of a preeclamptic placenta. B) The maternal side of a preeclamptic placenta.*

Placental morphology of the fetal side

Representative overview images of a cryo-section from the fetal side of a normal placenta are presented in Figure 11. In Figure 11A, the cryo-section is magnified 10×. Figure 11B shows the squared region in A at 20× magnification, where fetal villi with syncytiotrophoblasts (ST), fetal capillaries (FC) and syncytial knots (SK) are identified.

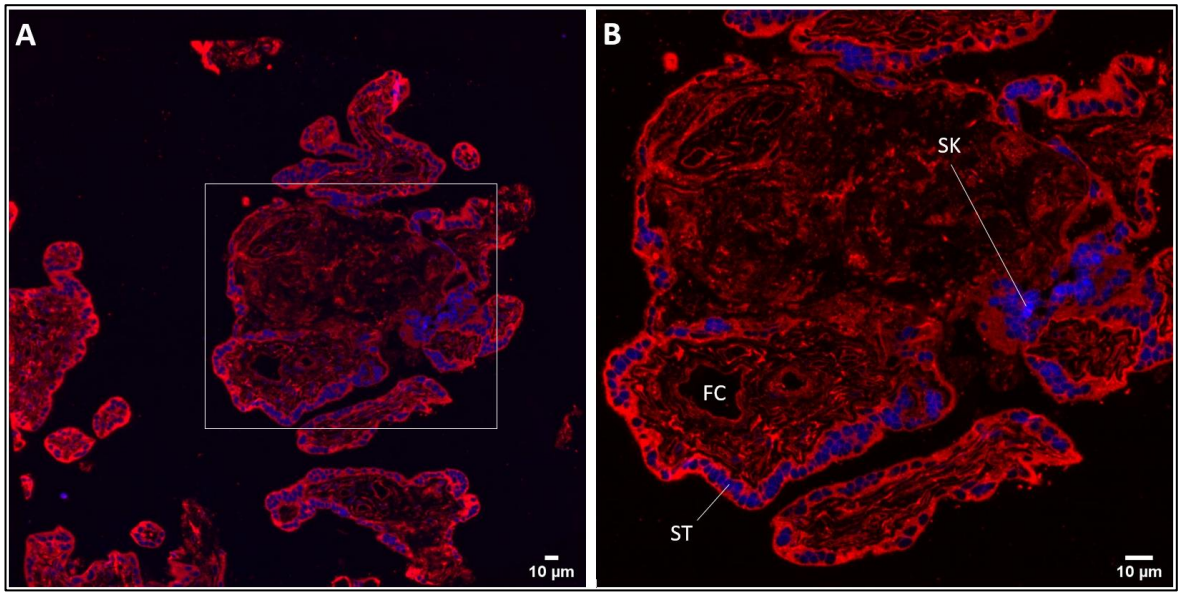

Figure 11: Cryo-sections of the fetal side of a normal placenta. *Cell membranes (red) are stained with CellMask™ Orange and nucleic acids (blue) are stained with 4',6-diamidino-2-phenylidole, dihydrochloride. A) Overview image at 10× magnification. B) The squared area in A at 20× magnification, showing a fetal capillary (FC), syncytiotrophoblasts (ST) and a syncytial knot (SK).*

Approximately the same region is magnified to 60× and the resolution is increased using deconvolution as presented in Figure 12A. The squared region in A is enlarged in Figure 12B, where a fetal capillary and syncytiotrophoblasts are be identified.

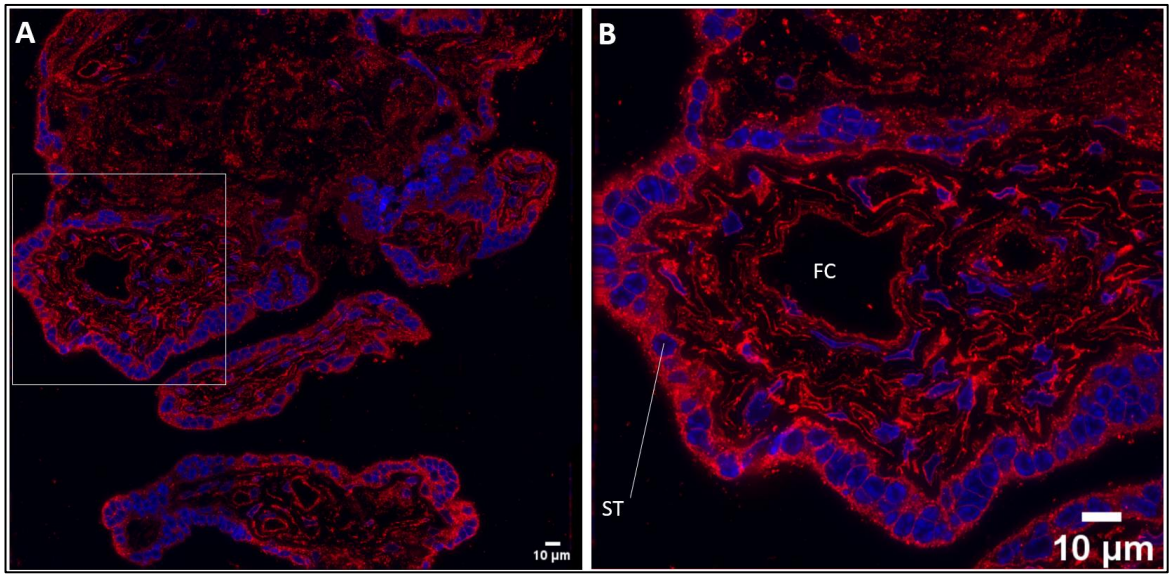

Figure 12: Cryo-sections of the fetal side of a normal placenta*. Cell membranes (red) are stained with CellMask™ Orange and nucleic acids (blue) are stained with 4',6-diamidino-2-phenylidole, dihydrochloride. A) A mosaic using deconvolution. B) Enlargement of the squared area in A, showing syncytiotrophoblasts (ST) and a fetal capillary (FC).*

The resolution of a smaller region of the villi is further increased using SIM and is presented in Figure 13A. The squared region in A is enlarged and presented in Figure 13B, showing a fetal capillary and syncytiotrophoblasts.

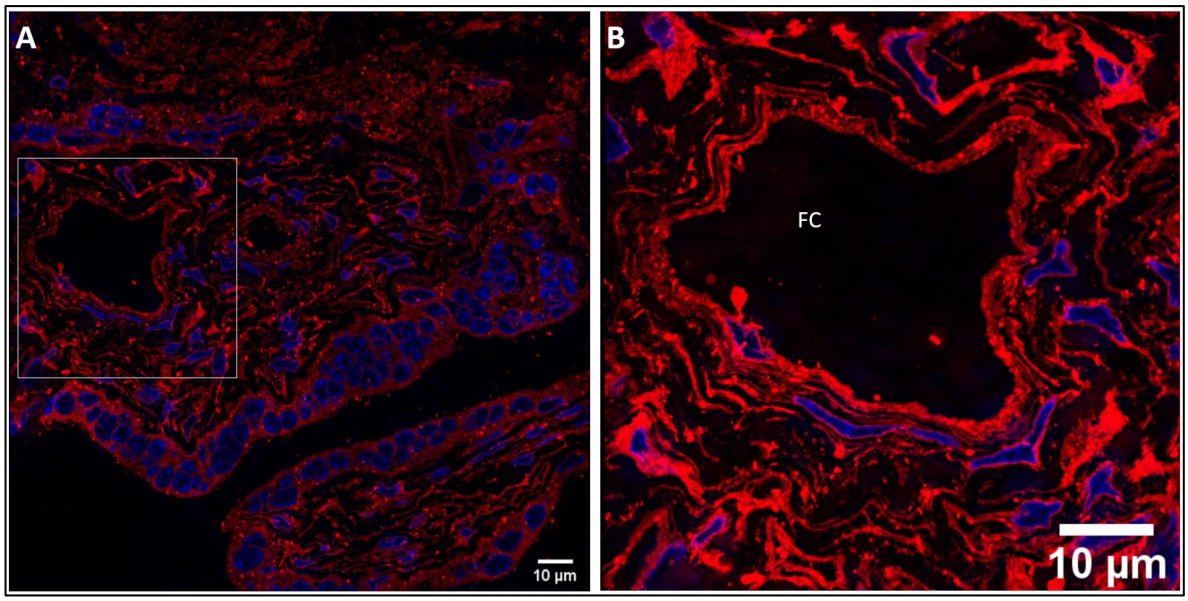

Figure 13: Cryo-sections of the fetal side of a normal placenta. *Cell membranes (red) are stained with CellMask™ Orange and nucleic acids (blue) are stained with 4',6-diamidino-2-phenylidole, dihydrochloride. A) A mosaic using structured illumination microscopy. B) Enlargement of the squared area in A, showing a fetal capillary (FC).*

Representative overview images of a cryo-section of the fetal side of a preeclamptic placenta are presented in Figure 14. In Figure 14A, the cryo-section is magnified 10×. In Figure 14B shows the squared region in A at 20× magnification, where fetal villi defined by the outer syncytiotrophoblasts and fetal capillaries are identified.

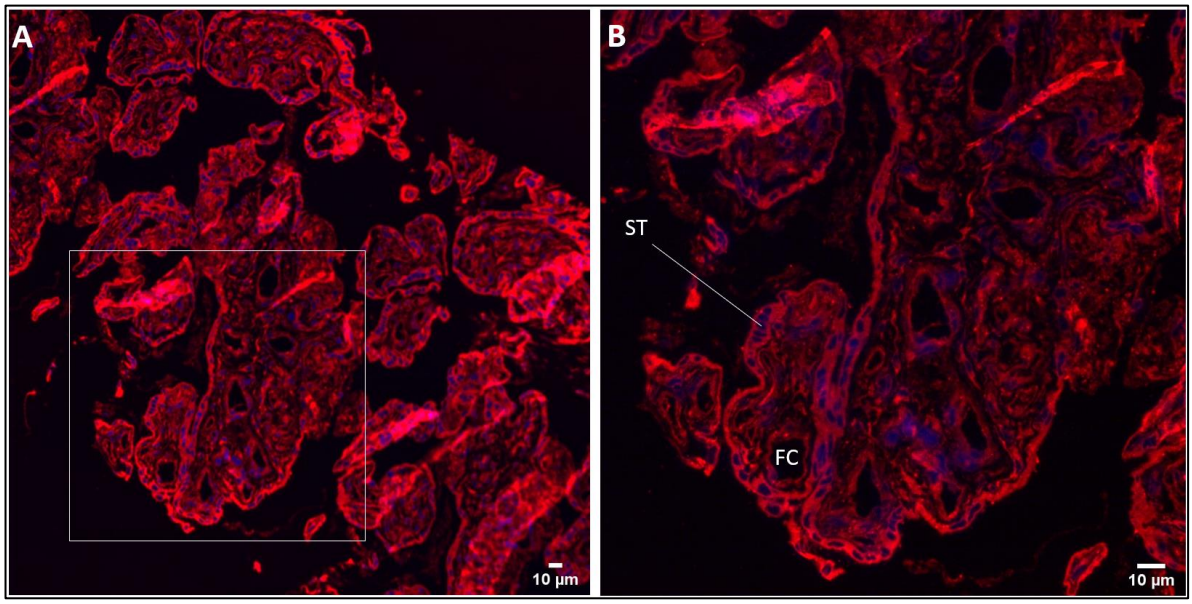

Figure 14: Cryo-sections of the fetal side of a preeclamptic placenta. *Cell membranes (red) are stained with CellMask™ Orange and nucleic acids (blue) are stained with 4',6-diamidino-2-phenylidole, dihydrochloride. A) Overview image at 10× magnification. B) The squared area in A at 20× magnification, showing fetal capillaries (FC) and syncytiotrophoblasts (ST).*

Approximately the same region is magnified to 60× magnification and the resolution is increased using deconvolution and is presented in Figure 15A. The squared region in A is enlarged in Figure 15B, where fetal capillaries and syncytiotrophoblasts are be identified.

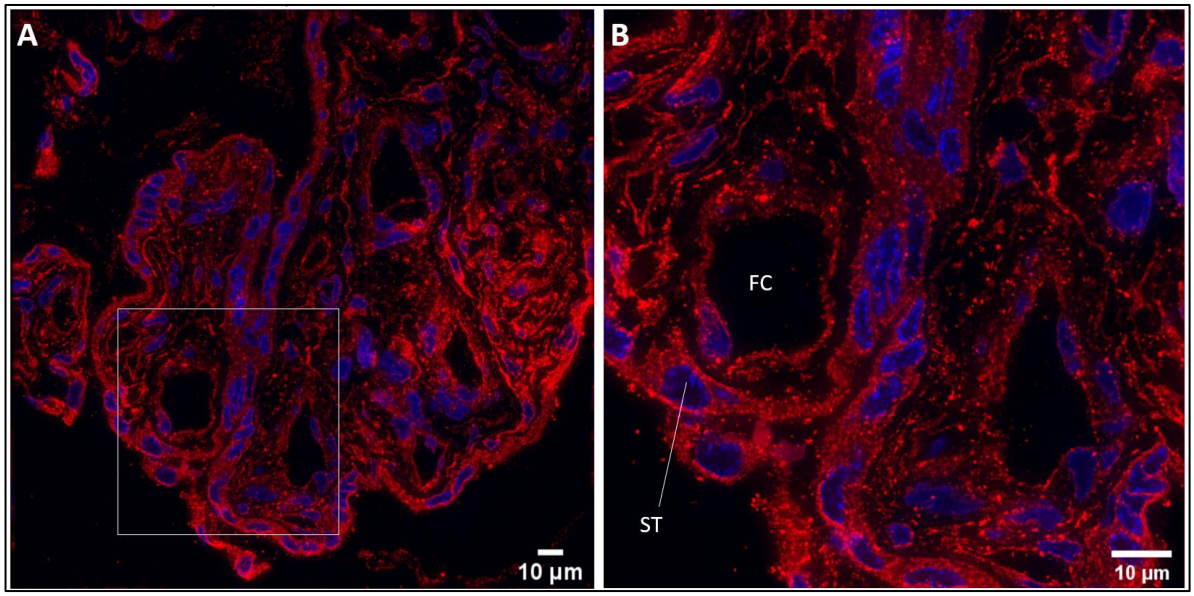

Figure 15: Cryo-section of the fetal side of a preeclamptic placenta. *Cell membranes (red) are stained with CellMask™ Orange and nucleic acids (blue) are stained with 4',6-diamidino-2-phenylidole, dihydrochloride. A) A mosaic using deconvolution. B) Enlargement of the squared area in A, showing fetal capillaries (FC), syncytiotrophoblasts (ST) and bright red structures.*

The resolution of a smaller region of the villi is further increased using SIM and is presented in Figure 16A. The squared region in A is enlarged and presented in Figure 16B, showing fetal capillaries, syncytiotrophoblasts and brighter red structures. The red structures range from about 100 nm to 500 nm in size.

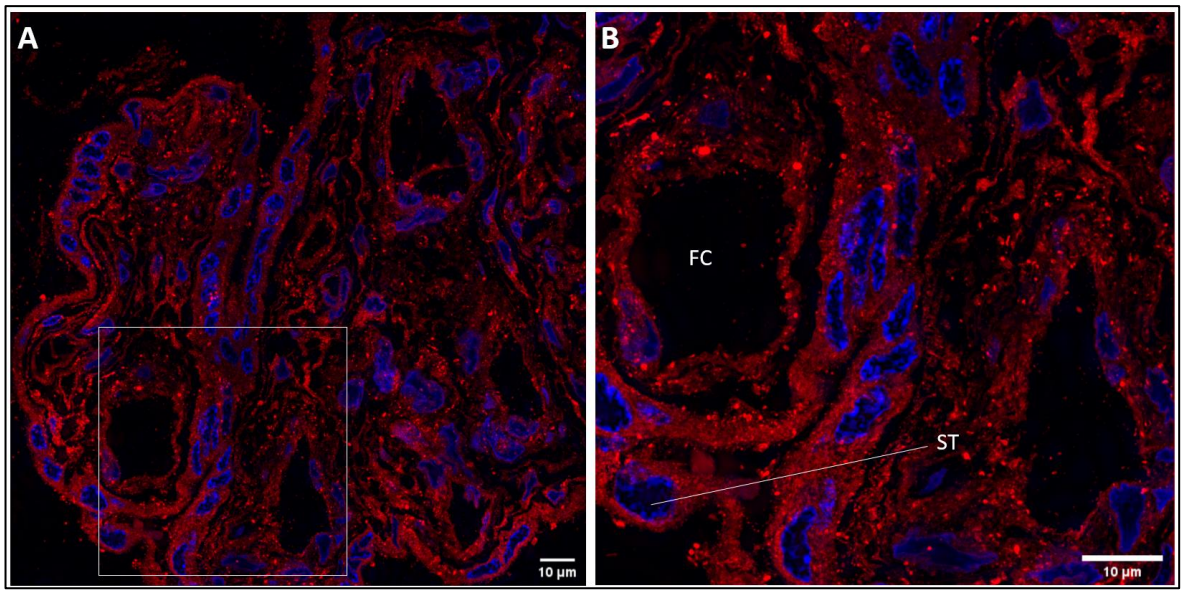

Figure 16: Cryo-section of the fetal side of a preeclamptic placenta. *Cell membranes (red) are stained with CellMask™ Orange and nucleic acids (blue) are stained with 4',6-diamidino-2-phenylidole, dihydrochloride. A) A mosaic using structured illumination microscopy. B) Enlargement of the squared area in A, showing fetal capillaries (FC), syncytiotrophoblasts (ST) and bright red structures.*

Table 19 summarises the structures identified in normal- and preeclamptic sections from the fetal side. Fetal capillaries, syncytial knots and syncytiotrophoblasts were found in both the normal- and preeclamptic sections, whereas brighter red structures only were identified in preeclamptic sections. Comparisons of the preeclamptic sections resulted in the identification of the same structures and similar morphology. The same applied for comparisons of the normal sections.

Table 19: Structures visualised in the fetal side of the normal- and preeclamptic placental sections. *"+" denotes that the structure is found in the sections, whereas "-" denotes that the structure is not found in the sections. Comparisons of the fetal sections in the normal- and preeclamptic group revealed the same structures. The table is a summary of the findings.*

Fetal side		
	Normal (n=3)	Preeclamptic (n=3)
Brighter, red structures	-	+
Fetal capillaries	+	+
Syncytial knots	+	+
Syncytiotrophoblasts	+	+

Placental morphology of the maternal side

Representative overview images of a cryo-section of the maternal side of a normal placenta are presented in Figure 17. In Figure 17A, the cryo-section is magnified 10×. Figure 17B shows the squared region in A at 20× magnification, where extravillous trophoblasts (ET), maternal capillaries (MC) and fetal capillaries are identified.

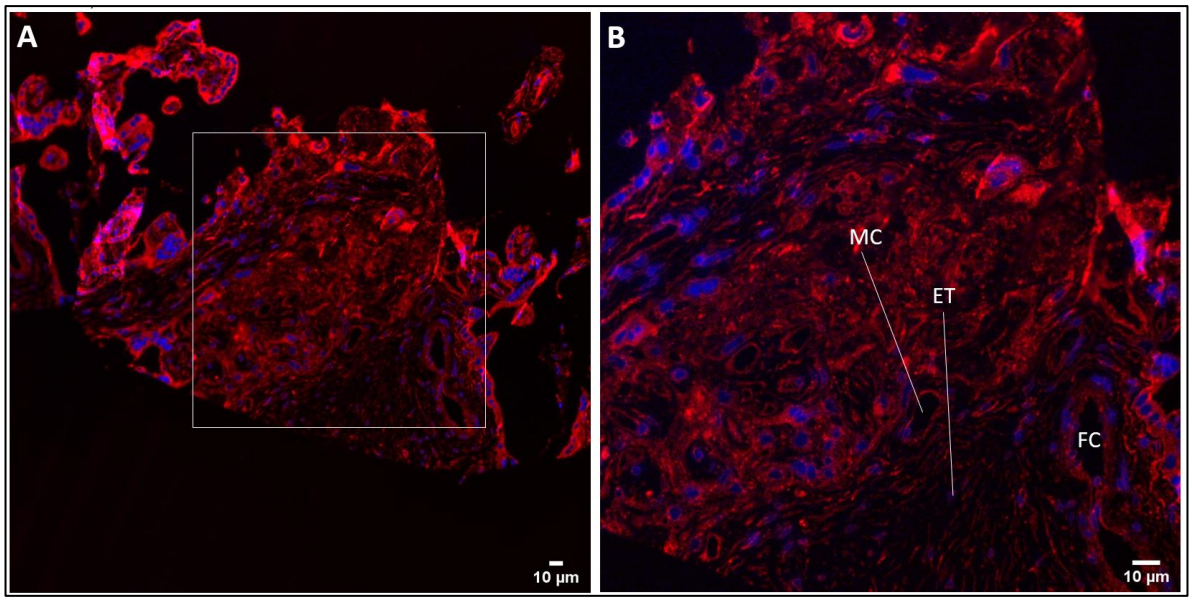

Figure 17: Cryo-section of the maternal side of a normal placenta. *Cell membranes (red) are stained with CellMask™ Orange and nucleic acids (blue) are stained with 4',6-diamidino-2-phenylidole, dihydrochloride. A) Overview image at 10× magnification. B) The squared area in A at 20× magnification, showing maternal capillaries (MC), fetal capillaries (FC) and extravillous trophoblasts (ET).*

Approximately the same region is magnified to 60× and the resolution is increased using the deconvolution and SIM as presented in Figure 18A and B, respectively. In both images, extravillous trophoblasts, maternal capillaries and fetal capillaries are identified.

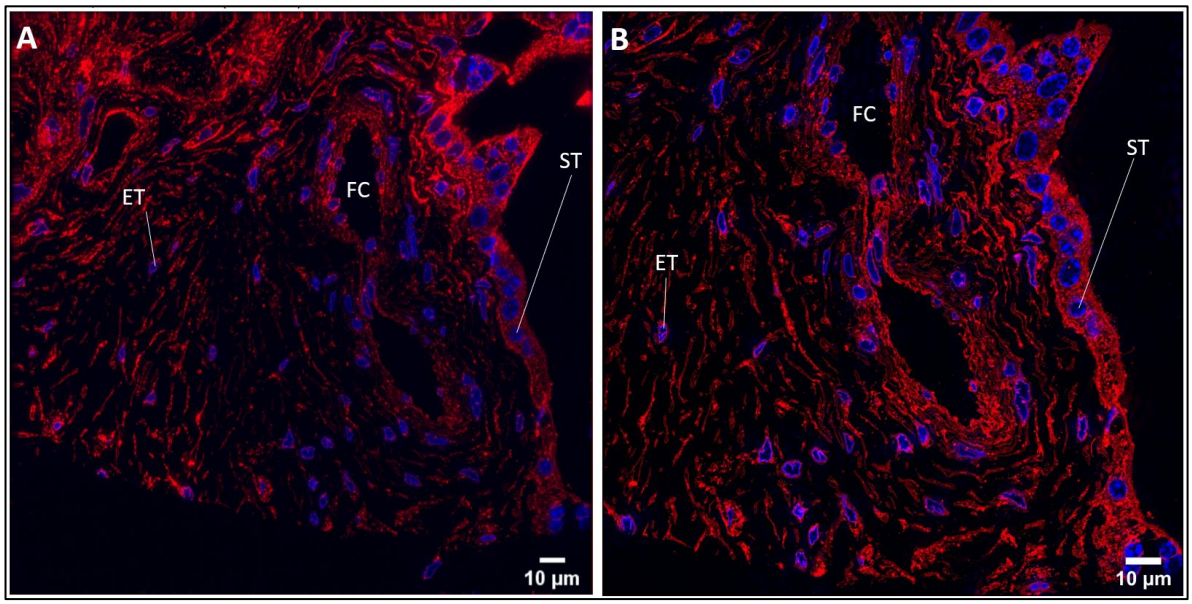

Figure 18: Cryo-section of the maternal side of a normal placenta*. Cell membranes (red) are stained with CellMask™ Orange and nucleic acids (blue) are stained with 4',6-diamidino-2-phenylidole, dihydrochloride. A) A mosaic using deconvolution, showing extravillous trophoblasts (ET), fetal capillaries (FC) and syncytiotrophoblasts (ST). B) A mosaic using structured illumination microscopy, showing extravillous trophoblasts, fetal capillaries and syncytiotrophoblasts.*

Representative overview images of a cryo-section of the maternal side of a preeclamptic placenta are presented in Figure 19. In Figure 19A, the cryo-section is magnified 10×. Figure

19B shows the squared region in A at 20× magnification, where extravillous trophoblasts (ET) are identified.

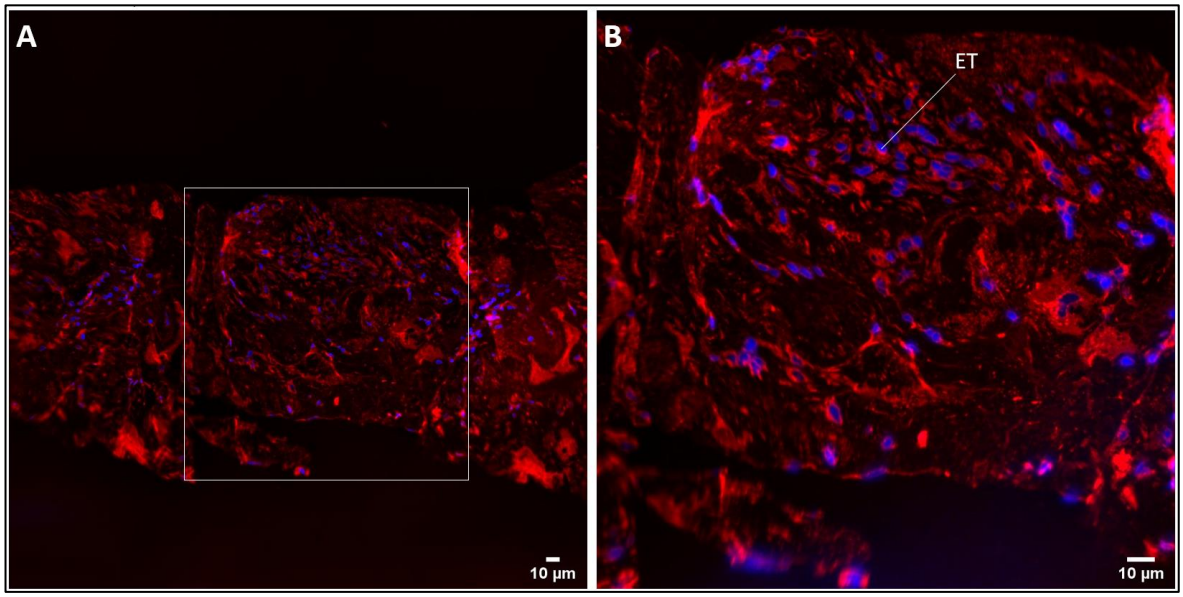

Figure 19: Cryo-section of the maternal side of a preeclamptic placenta. *Cell membranes (red) are stained with CellMask™ Orange and nucleic acids (blue) are stained with 4',6-diamidino-2-phenylidole, dihydrochloride. A) An overview image at 10× magnification. B) The squared area in A at 20× magnification, showing extravillous trophoblasts (ET).*

Approximately the same region is magnified to 60× and the resolution is increased using the deconvolution and SIM as presented in Figure 20A and B, respectively. In both images, extravillous trophoblasts are identified.

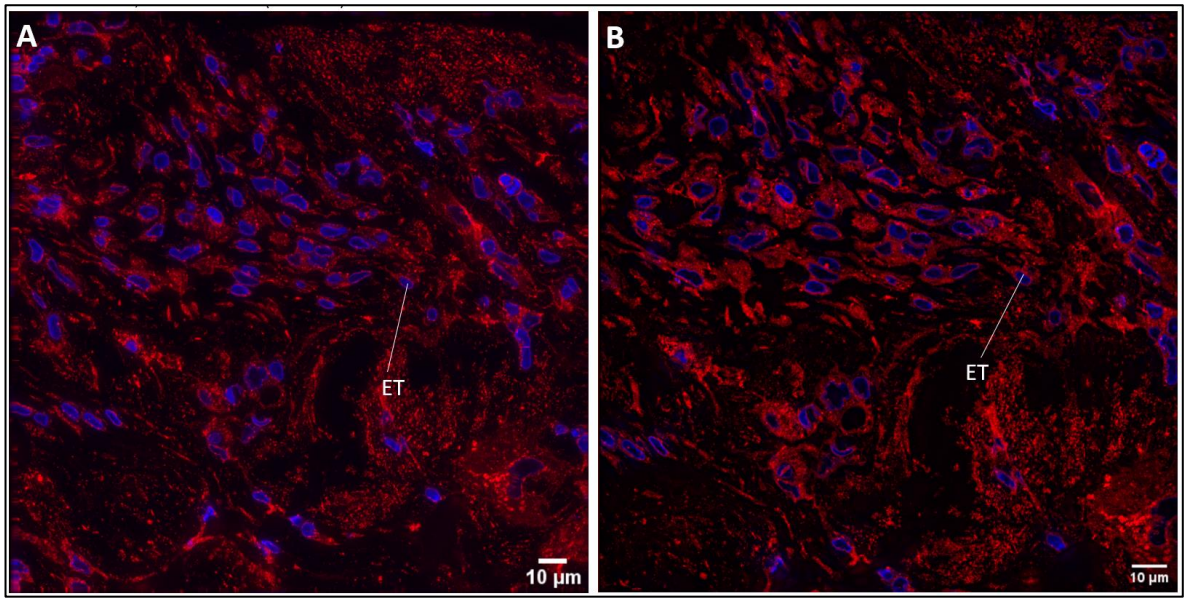

Figure 20: Cryo-section of the maternal side of a preeclamptic placenta. *Cell membranes (red) are stained with CellMask™ Orange and nucleic acids (blue) are stained with 4',6-diamidino-2-phenylidole, dihydrochloride. A) A mosaic using deconvolution, showing extravillous trophoblasts (ET). B) A mosaic using structured illumination microscopy, showing extravillous trophoblasts (ET).*

Table 20 summarises the structures identified in normal- and preeclamptic sections from the maternal side. Extravillous trophoblasts were found in both normal- and preeclamptic sections, whereas maternal capillaries were only found in the normal cryo-sections. Comparisons of the preeclamptic sections resulted in the identification of the same structures and similar morphology. The same applied for comparisons of the normal sections.

Table 20: Structures visualised in the maternal side of the normal- and preeclamptic placental sections. *"+" denotes that the structure is found in the sections, whereas "-" denotes that the structure is not found in the sections. Comparisons of the maternal sections in the normal- and preeclamptic group revealed the same structures. The table is a summary of the findings.*

Maternal side		
	Normal (n=3)	Preeclamptic (n=3)
Extravillous trophoblasts	+	+
Maternal capillaries	+	-

Oxidative stress study

Total antioxidant capacity in normal- and preeclamptic placental tissue

TAC of the tissue samples was determined by measuring the ABTS radical scavenging activity by the antioxidants present in the tissue samples. The radical scavenging activity was measured spectrophotometrically at 730 nm wavelength and the OD_{730} of each sample was compared to the standard curve of ascorbic acid.

The standard curve for the antioxidant capacity of ascorbic acid was prepared by measuring the ABTS radical scavenging activity by the known concentrations of ascorbic acid, ranging from 0–10 ug/mL. The TAC of the tissue samples is expressed as ascorbic acid equivalent antioxidant activity guided by the standard curve as shown in Figure 21.

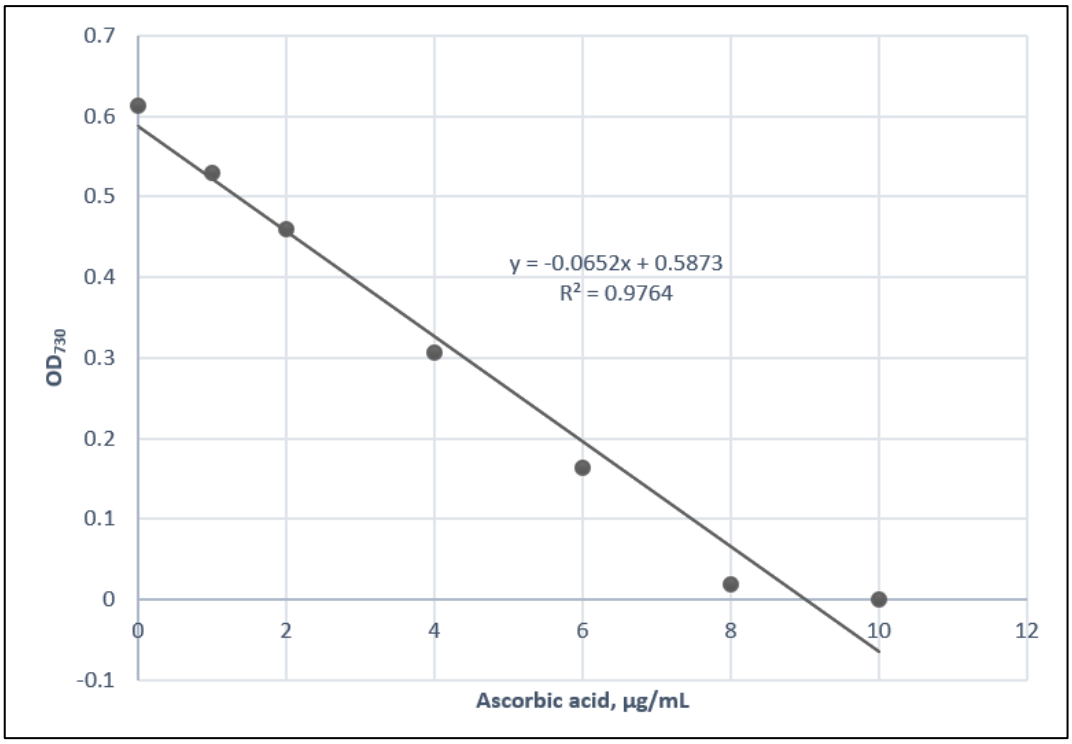

Figure 21: The standard curve showing the ABTS radical scavenging activity of known concentrations of ascorbic acid. *Results are presented as the mean of three independent measurements. By using linear regression, the equation of the line is y=-0.0652x+0.5873 and the regression coefficient (R^2) for the line is 0.98. The standard curve was used to determine the ascorbic acid equivalent concentration of total antioxidant capacity in the placental tissue samples, using the average optical density at 730 nm wavelength of the three independent measurements for each sample.*

Table 21 shows the average OD_{730}, TAC expressed as µg ascorbic acid/mg placental tissue and *p*-value for the normal and- preeclamptic tissue samples, for both the maternal and fetal side. The average OD_{730} was used to calculate the average TAC in the same placental samples using the standard curve for ascorbic acid. There is no statistically significant difference between the antioxidant capacities of the normal- and preeclamptic placental samples, neither on the maternal or the fetal side.

Table 21: The total antioxidant activity (TAC) of normal- and preeclamptic placental tissue samples. *Results are presented as the mean of the three normal- and preeclamptic samples, where each sample had three independent measurements.*

Side	Sample	Average OD_{730}	TAC (µg ascorbic acid equivalent/mg placental tissue) ± SD	*p*-value
Fetal	Normal	0.28623	4.62 ± 0.59271	0.23344
	Preeclamptic	0.32296	4.05 ± 0.37220	
Maternal	Normal	0.27042	4.86 ± 0.53226	0.82927
	Preeclamptic	0.27534	4.78 ± 0.22279	

Oxidative stress in normal- and preeclamptic placental tissue

The oxidative stress of the tissue samples was determined by measuring the MDA content in the placental tissue samples. After the reaction with TBA, OD_{532} of each sample was compared to the standard curve of MDA.

The standard curve of MDA content was prepared by measuring the OD_{532} of known MDA content, ranging from 0 to 20 nM after the reaction with TBA. The oxidative stress of the tissue samples are expressed as the MDA content guided by the standard curve as shown in Figure 22.

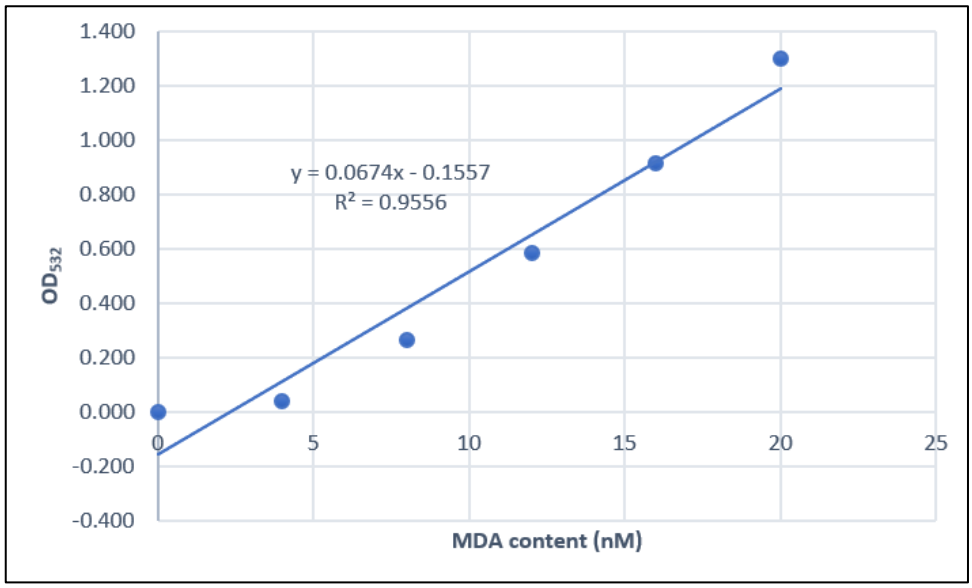

Figure 22: The standard curve for malondialdehyde (MDA). *Results are expressed as mean of two independent measurements. By using linear regression, the equation of the line is y=0.0674x-0.1557 and the regression coefficient (R^2) for the line is 0.96. The standard curve was used to determine the amount of MDA in the placental tissue samples using the average optical density at 532 nm wavelength for the two independent measurements for each sample.*

Table 22 shows the average OD_{532}, MDA content in nM/mg placental tissue and *p*-value for the normal- and preeclamptic tissue samples, both the maternal- and fetal side. The average OD_{532} was used to calculate the average MDA content in the placental tissue samples using the standard curve for MDA content. There is no significant difference between the MDA content in the normal- and preeclamptic samples, neither on the maternal- or the fetal side.

Table 22: Oxidative stress expressed as the MDA concentration in normal- and preeclamptic placental tissue samples. *Results are presented as the mean ± standard deviation (SD) of the three normal- and preeclamptic samples, where each sample had two independent measurements.*

Side	Sample	Average OD_{532}	Oxidative stress (nM MDA/mg placental tissue) ± SD	*p*-value
Fetal	Normal	0.435	8.77 ± 0.932	0.113
	Preeclamptic	0.521	10.03 ± 0.543	
Maternal	Normal	0.407	8.35 ± 0.704	0.735
	Preeclamptic	0.430	8.70 ± 1.516	

Discussion

Clinical parameters

Mean arterial pressure (MAP) and arterial cord blood Base Excess had a significant difference (*p*=0.014) between the two groups. MAP was measured prior to labour or caesarean section and was significantly higher in the women with PE compared to the normal women. This observation agrees with the main theory of PE saying that expansion of the spiral arteries diameter by the extravillous trophoblasts are incomplete (21).

Arterial blood pressure base excess was the only parameter with a significant difference (*p*=0.048) between the umbilical cords from normal- and preeclamptic placentas. The umbilical cord has three blood vessels: one large vein transporting oxygenated blood to the fetus, and two smaller arteries transporting deoxygenated blood and other metabolic waste products from the fetus (71). Venous cord blood reflects the combined effect of the maternal acid-base status. Maternal factors as hypertension may lead to decreased uterine blood flow. Uteroplacental factors as placental infarction or dysfunction may also cause abnormal fetal oxygenation during labour (65). The pH, base excess and pCO_2 (acid-base status) of arterial blood flowing through the umbilical cord provides valuable objective evidence of the metabolic condition of neonates at birth.

The number of caesarean sections were significantly higher (*p*=0.000) in the preeclamptic group compared to the normal group. This is as expected since PE usually occurs preterm, meaning the fetus is not fully developed. Therefore, the pregnancy is maintained as long as

possible to enhance the fetal outcome (65). Caesarean sections are therefore performed when the maternal condition is critical, as the only current cure for PE is removal of the placenta.

Other measured clinical patient parameters did not show a significance difference ($p \geq 0.05$), neither between the mothers nor the neonates. However, there was expected to be significant differences in e.g. BMI, maternal age and nulliparous, as these factors are thought to increase the prevalence of PE (6). Because proteinuria is one of the first signs of PE, the urine of the women in the normal control group were not analysed as they had no signs of proteinuria in their routine controls.

Implementation and optimisation of methods for morphology studies

The resolution of SIM is 100 nm compared to 50 pm in the transmission electron microscope (TEM) (63, 72). SIM is a versatile method where many fluorophores may be used in one experiment, allowing a detailed analysis of one section (63). TEM on the other hand, only allows using a few different sized gold labelled particles in one section (72). Also, high-resolution fluorescent microscopy as SIM is a cheaper and quicker method to perform than TEM.

In 2018, a Master project were conducted at the Optical Nanoscopy Research Group, comparing the image quality of cryo-sections and formalin-fixed paraffin-embedded (FFPE) sections from liver tissue using high-resolution microscopy (73). The previous Master project found that ultrathin cryo-sections allow better contrast images compared to FFPE sections. There are at least two reasons for this; first, cryo-sections are generally thinner than FFPE sections, leading to less out-of-focus information. Second, cryopreservation allows for ultrastructural preservation and better antigen accessibility for fluorescent markers as compared to FFPE samples (74). In addition to these findings, cryo-sections are easier and more time effective to label as it is not necessary to first embed the tissue piece in paraffin, followed by deparaffinisation steps prior to labelling. Because of this, cryo-sections were used in favour of FFPE in this thesis.

Prior to this study, no established protocol for collection and preservation of placental tissue for high-resolution microscopy of cryo-sections existed. The collection and fixation protocol were based on knowledge of fluorescent- and electron microscopy of placental and other tissues. This was used to further optimise the protocol for cryopreservation of placenta for high-resolution microscopy. First, fixation was performed following two different approaches; one using glutaraldehyde and formaldehyde, and one using only formaldehyde. Sections preserved using the fixative containing both glutaraldehyde and formaldehyde were not as evenly stained as the sections preserved in the fixative containing only formaldehyde. Therefore, the fixative containing only formaldehyde was used.

Placental tissue has chorion villi submersed in the maternal blood in the intervillous space (75). Bernhard and Virion found in 1971 that tissues are better preserved when it is immersed in gelatine (76). This coincides with our previous experience from other collection and preservation protocols. When the tissue is immersed in gelatine, cavities are filled, and the tissue is prevented from collapsing. Placental tissue samples that were used in the previous Master project were not immersed in gelatine prior to freezing, resulting in a distorted placental morphology. Also, the previously cryo-preserved tissues were fixed using various fixatives, making implementation of a labelling protocol difficult. Implementation of a protocol was difficult as there are many various parameters to optimise.

In the previous Master study, it was found that cryo-sections did not adhere to the cover glass during the washing and labelling steps when it was not coated with poly-L-lysine (73). Therefore, only poly-L-lysine coated cover glasses were used in this study. The method used to label cryo-sections from liver in the previous Master project, and experience with labelling procedure of FFPE sections and sections for electron microscopy was used as basis for the optimised labelling method of placental cryo-sections. First, the methyl cellulose was not fully removed, leading to it being a hazy layer over parts of the sections, making it difficult to focus in the microscope. The methyl cellulose residues also lead to an unsuccessful labelling with CMO and DAPI. As a solution, the poly-L-lysine coated cover glasses with the cryo-sections were cooled down on a metal plate prior to washing, leading to an easier removal of the methyl cellulose and cryo-sections that were better labelled. Still, some autofluorescence that

might affect the imaging were detected. Because of this, the blocking solution was changed from normal goat serum (1 %) to BSA (1 %). Thereafter, the optimal concentration of CMO and DAPI were found by labelling different sections with different concentrations of CMO and DAPI. At initial phases of the study, it was also discovered that some parts of the sections were in focus whereas other parts were not. To ensure correct flatness of the focal plate, a six-edged nut was placed on top of the cover glasses while the mounting medium hardened.

During this study, there has been made attempts to label the cryo-sections with antibodies. Two trophoblast-specific antibodies were chosen: laeverin and HLA-G antibody (77, 78). Different batches of both primary- and secondary antibodies were used without success. Further investigations and optimisations are needed to successfully label cryo-sections with antibodies. For later experiments, longer incubation time for the primary antibody, using a different blocking solution and higher concentrations of the antibodies can be tested.

Morphological investigation using high-resolution microscopy

As shown in Figure 9 and Figure 10, neither sections from normal or preeclamptic placentas showed significant autofluorescence values that could affect or interfere with imaging of the stained sections.

Because SIM has a higher resolution than deconvolution, SIM was used for morphological analysis (63). All normal- and preeclamptic sections confirm the expected morphology of placental tissue, having symmetrical nuclei and uniform staining with both CMO and DAPI, indicating that the tissue was well preserved and that suitable concentrations of CMO and DAPI were used. Comparison of normal- and preeclamptic cryo-sections within the group disclosed that sections from all patients had the same structures. However, one patient had early PE and the labour was induced preterm (gestational week 27+3). Therefore, the structures less developed in these tissues.

A series of artefacts were discovered during this study, which could have been introduced during sectioning, preparation of the sections or microscopy. Some sections had stripes occurring from notches in the knife used to section the tissue sample and are not presented in the thesis. When these stripes affected the ability of analysing the images, new sections

were made. Virtually all sections had some folds, some more than others. This occurred after sectioning, when the tissue section was transferred to the poly-L-lysine-coated cover glass. The folded regions were not used for investigative purposes and are therefore not presented in the thesis. Sections with too much folds were discarded and replaced by new sections. During preparation, the ultrathin cryo-sections are invisible to the naked eye, making it impossible to inspect them during the various washing and labelling steps of the preparation. In cases were the section was accidentally touched with absorbent paper, tears and rifts may occur, affecting the overall morphology of the tissue, thus, requiring new sections to be made.

Artefacts can be introduced during microscopy, such as oil mismatch. It was ensured that oil mismatch did not occur by checking the PSF in the orthogonal view of the software, to see whether symmetrical shapes occurred (Figure 6). If unsymmetrical shapes occurred, the oil was changed accordingly. In addition, some sections may be unevenly placed on the cover glass, leading to some structures being in focus, whereas other structures are not in focus. As the overall aim of the thesis was to implement a method for high-resolution microscopy of placental cryo-sections, the structures were not quantified. Prolonged exposure of light on the samples leads to photobleaching of the fluorophores and results in diminishing fluorescence. This occurred with the sample of the normal section from the maternal side presented Figure 18A and B. When the section was imaged in the fluorescence microscope (Figure 17B), maternal capillaries were visualised, whereas when the same region was imaged using SIM, the maternal capillaries could not be visualised (Figure 18A and B).

On the fetal side, the same structures were visualised in both the normal- and preeclamptic samples (Table 19). In both the normal- and preeclamptic fetal sections, the syncytiotrophoblasts were evenly spread in the syncytium. All sections used for analysing purposes were uniformly stained.

Bright red structures in the cytoplasm are seen in all preeclamptic sections on the fetal side (Figure 16B), but are not found in the normal sections from the fetal side (Figure 13B). Their size range from 100 nm to 500 nm in diameter; they might be EVs, according to their size (79). Organelles such as mitochondria are excluded since they have a diameter ranging between 0.5-1 µm (80). Previous studies have shown an abundance of trophoblastic

fragments, vesicles and cell free DNA and RNA in the maternal circulation during pregnancy (81). Compared to normal pregnancies, more are shed into the maternal circulation in PE (50, 81). The presumed EVs found in this study may be a biomarker of PE, and thus need to be investigated further with EV specific markers like vascular endothelial growth factor receptor 1 (Flt-1) and endoglin (82).

When comparing the fetal side of the normal- and preeclamptic samples, it may seem to be more syncytial knots in the preeclamptic samples. Syncytial knots are a cluster of syncytial nuclei on the outer surface of a placental villi and a sign of syncytial damage, occurring when syncytial nuclei progress to apoptosis and aggregates (83). Such morphological changes in syncytiotrophoblasts may lead to reduction of the placental barrier, allowing leakage of fetal antigen into maternal circulation, thus, increasing the immune response and expose the fetus to harmful agents (84). Previous studies have found that there are two times more syncytial knots in placentas from women with PE compared to normal women (85). Fragments of the syncytial knots can be shed into the intervillous space and enter the maternal circulation. The number of syncytial knots increases with gestational age (86). Therefore, a morphological comparison of normal- and preeclamptic placentas should be carried out in women with the same gestational age at delivery.

On the maternal side, extravillous trophoblasts, syncytiotrophoblasts and both maternal and fetal capillaries were identified (Table 20). The maternal side of the normal- and preeclamptic sections show similar morphology. It appears to be more scattered nuclei in the normal sections in general than the preeclamptic sections. The scattered nuclei may be extravillous trophoblasts as they are surrounded by a thicker cell membrane, containing glycocalyx, than other trophoblastic cells (87). However, to confirm this hypothesis, extravillous trophoblast-specific marker must be used. Extravillous trophoblasts are differentiated trophoblasts that invade the decidua during the second trimester, increasing the diameter of the maternal arteries supplying the placenta with maternal blood, thereby adapting to the nutritional needs of the growing fetus (20).

No maternal capillaries were identified in the preeclamptic sections from the maternal side, making a comparison impossible. The reason for this may be because the prepared sections

originate from the outer rim towards the fetal side of the collected tissue piece. Therefore, maternal capillaries can appear when more sections from parts deeper into the maternal side are prepared. For the same reason, fetal capillaries and parts of fetal villi such as syncytiotrophoblasts appears in some of the maternal sections as well. It is impossible to ensure that the orientation of each section is equal and achieve the same structures. There are also individual differences between women. However, individual differences were not observed in this study, probably because of a low number of samples. Also, if more markers are used to label the sections, individual differences in and between the normal- and preeclamptic group are easier to detect.

Even though all the samples were collected at approximately the same distance from the umbilical cord, the pieces that are stored are very small and are randomly selected for sectioning. In a larger study, more sections from each patient could be prepared, increasing the possibility to visualise more structures and detect differences between the groups. The women included in the study should also have been matched for gestational age to ensure approximately equal development of the placenta. As the primary aim was to implement a method for collection, preservation and labelling, a limited number of sections were prepared for morphological analysis when the method was optimised.

Total antioxidant capacity and oxidative stress study

To our knowledge, neither the method used to measure TAC or MDA have previously been used on placental tissue. Therefore, normal values are not established. Three parallels were used in the TAC assay, whereas two parallels were used in the MDA assay. In both assays, all measurements were stable (Appendix B and C). Because of this, the method seemed to work on placental tissue.

The TAC assay measures the tissue's ability of ROS elimination. All tissues have some antioxidative micronutrients such as vitamin C and vitamin E that eliminate ROS (88). Antioxidants scavenge ROS, meaning the more antioxidants in the tissue, the higher antioxidant capacity and higher rate of ROS elimination (30). In this study, there was no significant difference ($p \geq 0.05$) between the TAC of normal- and preeclamptic placental tissue.

However, the TAC of the normal tissue samples show a trend of being generally higher than the preeclamptic, both for the fetal and the maternal side (Table 21).

The MDA assay measures the MDA content of the samples. MDA is a product of lipid peroxidation after reacting with ROS, which occurs by oxidative stress. Therefore, a higher MDA value reflects an increased oxidative stress level in the tissue, whereas a lower MDA value reflects a lower oxidative stress level in the tissue. Although there was no significant difference ($p \geq 0.05$) between the normal- and preeclamptic tissue samples, there was a trend of the MDA content being higher in the preeclamptic samples, both for the fetal and maternal side (Table 22).

The oxidative stress and the TAC of a tissue is closely connected. It is found that pregnant women in general have increased levels of MDA compared to non-pregnant women (30). Also, previous studies have found that the TAC of preeclamptic placentas are lower than the TAC of normal placentas (89, 90). The TAC of the placental tissue in normal pregnant women increases as the oxidative stress in the tissue increases, thereby eliminating ROS and prevent increased oxidative stress (30). Pregnant women with PE have higher levels of MDA than normal pregnant women with the same gestational age, meaning this adaptation of the TAC does not occur in pregnant women with PE, leading to oxidative stress (30, 31). Since other studies have found that there is a significant difference in the TAC and MDA content between normal- and preeclamptic samples, the difference is probably found if more patients are included in the study.

Conclusions

The implemented protocol for collection and staining of placental tissue is well suited for investigating placental morphology using high-resolution microscopy, as the placental morphology is preserved, and the sections are evenly stained. The method is cheaper, more rapid and easier than TEM. In preeclamptic sections, there seemed to be more syncytial knots than in normal sections, in addition to bright red structures that may be EVs which were not found in normal sections. The methods used to determine TAC and MDA content can also be

used on placental tissue. No significant difference was found between the TAC and oxidative stress levels of normal- and preeclamptic placentas.

Future perspectives

The current method for sample preparation is well suited for high-resolution microscopy. However, the method should be further developed to include labelling of specific proteins, cell structures and cell types with antibody-conjugated fluorophores. This allows a more thorough investigation of placental morphology. By labelling more structures, morphological differences between normal- and preeclamptic placentas can be more easily detected and different subsets of placental cells can be identified. In addition, quantitative studies comparing the amount of EVs and syncytial knots may be performed on tissue sections from placentas of normal pregnancies and placentas from women with PE.

If the detected bright red structures are EVs, these are presumably secreted into the maternal circulation. To investigate whether this is the case, liquid biopsies from the maternal circulation can be performed. An advantage with this approach is that it is non-invasive and can be performed throughout the pregnancy. This approach can also be extended to include other biomarkers thought to be related to PE, such as microRNA, proteins and cell free fetal DNA. Over time, this result in the possibility of detecting pregnancies at risk of being affected with PE prior to disease onset.

References

1. Lindheimer MT, RN; Roberts, JM; Cunningham, FG; Chesley, L. Introduction, History, Controversies, and Definitions. Chesley's Hypertensive Disorders in Pregnancy. 4th ed. New York:Academic Press; 2015. p. 1-24.
2. Tranquilli AL, Dekker G, Magee L, Roberts J, Sibai BM, Steyn W, *et al*. The classification, diagnosis and management of the hypertensive disorders of pregnancy: A revised statement from the ISSHP. Pregnancy Hypertens. 2014;4(2):97-104.
3. Kintiraki E, Papakatsika S, Kotronis G, Goulis DG, Kotsis V. Pregnancy-Induced hypertension. Hormones (Athens). 2015;14(2):211-23.
4. Robert JM, August PA, Bakris G, Barton JR, Bernstein IM, Druzin M, *et al.* American College of Obstetricians and Gynecologists, Task Force on Hypertension in Pregnancy. Hypertension in pregnancy. Report of the American College of Obstetricians and Gynecologists' Task Force on Hypertension in Pregnancy. Obstet Gynecol. 2013;122(5):1122-31.
5. Weinstein L. Syndrome of hemolysis, elevated liver enzymes, and low platelet count: a severe consequence of hypertension in pregnancy. Am J Obstet Gynecol. 1982;142(2):159-67.
6. Chaiworapongsa T, Chaemsaithong P, Yeo L, Romero R. Pre-eclampsia part 1: current understanding of its pathophysiology. Nat Rev Nephrol. 2014;10(8):466-80.
7. North RA, McCowan LM, Dekker GA, Poston L, Chan EH, Stewart AW, *et al*. Clinical risk prediction for pre-eclampsia in nulliparous women: development of model in international prospective cohort. BMJ. 2011;342:d1875.
8. Bounds KR, Newell-Rogers MK, Mitchell BM. Four Pathways Involving Innate Immunity in the Pathogenesis of Preeclampsia. Front Cardiovasc Med. 2015;2:20.
9. Lisonkova S, Sabr Y, Mayer C, Young C, Skoll A, Joseph KS. Maternal morbidity associated with early-onset and late-onset preeclampsia. Obstet Gynecol. 2014;124(4):771-81.
10. Davis EF, Lazdam M, Lewandowski AJ, Worton SA, Kelly B, Kenworthy Y, *et al*. Cardiovascular risk factors in children and young adults born to preeclamptic pregnancies: a systematic review. Pediatrics. 2012;129(6):e1552-61.
11. Helsedirektoratet [Internet]. Oversikt over anbefalt innhold i svangerskapsomsorgen; 2018 [cited October 14th 2018]. Available from: https://www.helsedirektoratet.no
12. Chaiworapongsa T, Chaemsaithong P, Korzeniewski SJ, Yeo L, Romero R. Pre-eclampsia part 2: prediction, prevention and management. Nat Rev Nephrol. 2014;10(9):531-40.
13. Widmaier ER, Raff H, Strang KT. Reproduction. Vander's Human Physiology: The Mechanisms of Body Functions. 13th ed. New York: McGraw-Hill; 2014. p. 602-51.
14. Burton GJ, Fowden AL. The placenta: a multifaceted, transient organ. Philos Trans R Soc Lond B Biol Sci. 2015;370(1663):20140066.
15. Wang YZ, Zhao S. Structure of the Placenta. In: Vascular Biology of the Placenta [Internet]. San Rafael: Morgan & Claypool Life Science Publishers; 2010 [cited November 10th 2018]. Available from PubMed: https://www.ncbi.nlm.nih.gov/books/NBK53256
16. Moore KP, Persaud TVN. Placenta and Fetal Membranes. The Developing Human. 5th ed. Philadelphia: Elsevier; 1993. p. 99-130.

17. Zeldovich VB, Robbins JR, Kapidzic M, Lauer P, Bakardjiev AI. Invasive extravillous trophoblasts restrict intracellular growth and spread of Listeria monocytogenes. PLoS Pathog. 2011;7(3):e1002005.
18. Wang Y, Granger DN, Granger JP. Structure of the Placenta. Vascular Biology of the Placenta. 2nd. San Rafael: Morgan & Claypool Life Science Publishers; 2017. p. 13-6.
19. Fisher SJ, McMaster M, Roberts JM. The Placenta in Normal Pregnancy and Preeclampsia. In: Lindheimer MD, Roberts JM, Gary Cunningham F, editors. Chesley's Hypertensive Disorders in Pregnancy. 3rd ed. San Diego: Academic Press; 2009. p. 73-85.
20. Brosens I, Robertson WB, Dixon HG. The physiological response of the vessels of the placental bed to normal pregnancy. J Pathol Bacteriol. 1967;93(2):569-79.
21. Redman CW, Sargent IL. Latest advances in understanding preeclampsia. Science. 2005;308(5728):1592-4.
22. Brosens I, Renaer M. On the pathogenesis of placental infarcts in pre-eclampsia. J Obstet Gynaecol Br Commonw. 1972;79(9):794-9.
23. Redman CW. Current topic: pre-eclampsia and the placenta. Placenta. 1991;12(4):301-8.
24. Lunell NO, Nylund LE, Lewander R, Sarby B. Uteroplacental blood flow in pre-eclampsia measurements with indium-113m and a computer-linked gamma camera. Clin Exp Hypertens B. 1982;1(1):105-17.
25. Aouache R, Biquard L, Vaiman D, Miralles F. Oxidative Stress in Preeclampsia and Placental Diseases. Int J Mol Sci. 2018;19(5).
26. Pizzino G, Irrera N, Cucinotta M, Pallio G, Mannino F, Arcoraci V, *et al*. Oxidative Stress: Harms and Benefits for Human Health. Oxid Med Cell Longev. 2017;2017:8416763.
27. Gagné F. Oxidative Stress. In: Gagné F, editor. Biochemical Ecotoxicology. Oxford: Academic Press; 2014. p. 103-15.
28. Craige SM, Kant S, Keaney JF Jr. Reactive oxygen species in endothelial function - from disease to adaptation. Circ J. 2015;79(6):1145-55.
29. Rajendran P, Nandakumar N, Rengarajan T, Palaniswami R, Gnanadhas EN, Lakshminarasaiah U, *et al*. Antioxidants and human diseases. Clin Chim Acta. 2014;436:332-47.
30. Chiarello DI, Abad C, Rojas D, Toledo F, Vazquez CM, Mate A, *et al*. Oxidative stress: Normal pregnancy versus preeclampsia. Biochim Biophys Acta Mol Basis Dis. 2018; doi:11.1016/j.bbadis.2018.12.005.
31. Yang X, Guo L, Li H, Chen X, Tong X. Analysis of the original causes of placental oxidative stress in normal pregnancy and pre-eclampsia: a hypothesis. J Matern Fetal Neonatal Med. 2012;25(7):884-8.
32. Mittal M, Siddiqui MR, Tran K, Reddy SP, Malik AB. Reactive oxygen species in inflammation and tissue injury. Antioxid Redox Signal. 2014;20(7):1126-67.
33. Cindrova-Davies T, Spasic-Boskovic O, Jauniaux E, Charnock-Jones DS, Burton GJ. Nuclear factor-kappa B, p38, and stress-activated protein kinase mitogen-activated protein kinase signaling pathways regulate proinflammatory cytokines and apoptosis in human placental explants in response to oxidative stress: effects of antioxidant vitamins. Am J Pathol. 2007;170(5):1511-20.
34. Hennessy A, Pilmore HL, Simmons LA, Painter DM. A deficiency of placental IL-10 in preeclampsia. J Immunol. 1999;163(6):3491-5.

35. Arriaga-Pizano L, Jimenez-Zamudio L, Vadillo-Ortega F, Martinez-Flores A, Herrerias-Canedo T, Hernandez-Guerrero C. The predominant Th1 cytokine profile in maternal plasma of preeclamptic women is not reflected in the choriodecidual and fetal compartments. J Soc Gynecol Investig. 2005;12(5):335-42.
36. Keiser SD, Veillon EW, Parrish MR, Bennett W, Cockrell K, Fournier L, *et al*. Effects of 17-hydroxyprogesterone on tumor necrosis factor-alpha-induced hypertension during pregnancy. Am J Hypertens. 2009;22(10):1120-5.
37. LaMarca BB, Cockrell K, Sullivan E, Bennett W, Granger JP. Role of endothelin in mediating tumor necrosis factor-induced hypertension in pregnant rats. Hypertension. 2005;46(1):82-6.
38. Gadonski G, LaMarca BB, Sullivan E, Bennett W, Chandler D, Granger JP. Hypertension produced by reductions in uterine perfusion in the pregnant rat: role of interleukin 6. Hypertension. 2006;48(4):711-6.
39. Kharfi A, Giguere Y, Sapin V, Masse J, Dastugue B, Forest JC. Trophoblastic remodeling in normal and preeclamptic pregnancies: implication of cytokines. Clin Biochem. 2003;36(5):323-31.
40. Yoshizumi M, Perrella MA, Burnett JC Jr., Lee ME. Tumor necrosis factor downregulates an endothelial nitric oxide synthase mRNA by shortening its half-life. Circ Res. 1993;73(1):205-9.
41. Burton GJ, Yung HW, Cindrova-Davies T, Charnock-Jones DS. Placental endoplasmic reticulum stress and oxidative stress in the pathophysiology of unexplained intrauterine growth restriction and early onset preeclampsia. Placenta. 2009;30 Suppl A:S43-8.
42. Sano R, Reed JC. ER stress-induced cell death mechanisms. Biochim Biophys Acta. 2013;1833(12):3460-70.
43. Yang Y, Pei X, Jin Y, Wang Y, Zhang C. The roles of endoplasmic reticulum stress response in female mammalian reproduction. Cell Tissue Res. 2016;363(3):589-97.
44. Huppertz B, Kadyrov M, Kingdom JC. Apoptosis and its role in the trophoblast. Am J Obstet Gynecol. 2006;195(1):29-39.
45. Colombo M, Raposo G, Thery C. Biogenesis, secretion, and intercellular interactions of exosomes and other extracellular vesicles. Annu Rev Cell Dev Biol. 2014;30:255-89.
46. Muralidharan-Chari V, Clancy J, Plou C, Romao M, Chavrier P, Raposo G, *et al*. ARF6-regulated shedding of tumor cell-derived plasma membrane microvesicles. Curr Biol. 2009;19(22):1875-85.
47. Record M. Intercellular communication by exosomes in placenta: a possible role in cell fusion? Placenta. 2014;35(5):297-302.
48. Salomon C, Yee S, Scholz-Romero K, Kobayashi M, Vaswani K, Kvaskoff D, *et al*. Extravillous trophoblast cells-derived exosomes promote vascular smooth muscle cell migration. Front Pharmacol. 2014;5:175.
49. Sarker S, Scholz-Romero K, Perez A, Illanes SE, Mitchell MD, Rice GE, *et al*. Placenta-derived exosomes continuously increase in maternal circulation over the first trimester of pregnancy. J Transl Med. 2014;12:204.
50. Salomon C, Torres MJ, Kobayashi M, Scholz-Romero K, Sobrevia L, Dobierzewska A, *et al*. A gestational profile of placental exosomes in maternal plasma and their effects on endothelial cell migration. PLoS One. 2014;9(6):e98667.

51. Hulka B. Biological markers in epidemiology. Overwiev of biological markers. New York: Oxford University Press; 1990. p. 3-15.
52. Carlomagno N, Incollingo P, Tammaro V, Peluso G, Rupealta N, Chiacchio G, *et al*. Diagnostic, Predictive, Prognostic, and Therapeutic Molecular Biomarkers in Third Millennium: A Breakthrough in Gastric Cancer. Biomed Res Int. 2017;2017:7869802.
53. Cuffe JSM, Holland O, Salomon C, Rice GE, Perkins AV. Review: Placental derived biomarkers of pregnancy disorders. Placenta. 2017;54:104-10.
54. Chard T. Pregnancy tests: a review. Hum Reprod. 1992;7(5):701-10.
55. Gnoth C, Johnson S. Strips of Hope: Accuracy of Home Pregnancy Tests and New Developments. Geburtshilfe Frauenheilkd. 2014;74(7):661-9.
56. Conde-Agudelo A, Villar J, Lindheimer M. World Health Organization systematic review of screening tests for preeclampsia. Obstet Gynecol. 2004;104(6):1367-91.
57. Zeisler H, Llurba E, Chantraine F, Vatish M, Staff AC, Sennstrom M, *et al*. Predictive Value of the sFlt-1:PlGF Ratio in Women with Suspected Preeclampsia. N Engl J Med. 2016;374(1):13-22.
58. Rana S, Powe CE, Salahuddin S, Verlohren S, Perschel FH, Levine RJ, *et al*. Angiogenic factors and the risk of adverse outcomes in women with suspected preeclampsia. Circulation. 2012;125(7):911-9.
59. Giepmans BN, Adams SR, Ellisman MH, Tsien RY. The fluorescent toolbox for assessing protein location and function. Science. 2006;312(5771):217-24.
60. Sanderson MJ, Smith I, Parker I, Bootman MD. Fluorescence microscopy. Cold Spring Harb Protoc. 2014;2014(10):pdb top071795.
61. McNally JG, Karpova T, Cooper J, Conchello JA. Three-dimensional imaging by deconvolution microscopy. Methods. 1999;19(3):373-85.
62. Demmerle J, Innocent C, J North A, Ball G, Müller M, Miron E, *et al*. Strategic and practical guidelines for successful structured illumination microscopy. 2017;12(5):988-1010.
63. Chang BJ, Chou LJ, Chang YC, Chiang SY. Isotropic image in structured illumination microscopy patterned with a spatial light modulator. Opt Express. 2009;17(17):14710-21.
64. General Assembly of the World Medical Association. World Medical Association Declaration of Helsinki: ethical principles for medical research involving human subjects. J Am Coll Dent. 2014;81(3):14-8.
65. Staff AA, Andergaard AB, Henriksen T, Langesæter E, Magnussen E, Michelsen TM, *et al*. [Internet] Norwegian Gynecological Society. In: Hypertensive pregnancy complications and eclampsia; 2014 [cited August 7th 2019]. Available from https://www.legeforeningen.no.
66. Khong TY, Mooney EE, Ariel I, Balmus NC, Boyd TK, Brundler MA, *et al*. Sampling and Definitions of Placental Lesions: Amsterdam Placental Workshop Group Consensus Statement. Arch Pathol Lab Med. 2016;140(7):698-713.
67. Montanaro J, Gruber D, Leisch N. Improved ultrastructure of marine invertebrates using non-toxic buffers. PeerJ. 2016;4:e1860.
68. Tokuyasu KT. A study of positive staining of ultrathin frozen sections. J Ultrastruct Res. 1978;63(3):287-307.
69. Joraholmen MW, Skalko-Basnet N, Acharya G, Basnet P. Resveratrol-loaded liposomes for topical treatment of the vaginal inflammation and infections. Eur J Pharm Sci. 2015;79:112-21.

70. Songstad NT, Kaspersen KH, Hafstad AD, Basnet P, Ytrehus K, Acharya G. Effects of High Intensity Interval Training on Pregnant Rats, and the Placenta, Heart and Liver of Their Fetuses. PLoS One. 2015;10(11):e0143095.
71. Moore KP, Persaud TVN, Torchia, MG. Placenta and Fetal Membranes. The Developing Human. 10th ed. Philadelphia: Elsevier; 2015. p. 107-38.
72. Erni R, Rossell MD, Kisielowski C, Dahmen U. Atomic-resolution imaging with a sub-50-pm electron probe. Phys Rev Lett. 2009;102(9):096101.
73. Villegas L. Optical Nanoscopy of Tissue Sections [Master Thesis in Physics]: UiT - The Arctic University of Norway; 2018.
74. Tokuyasu KT. A technique for ultracryotomy of cell suspensions and tissues. J Cell Biol. 1973;57(2):551-65.
75. Wang YZ, Zhao S. Cell Types of the Placenta. In: Vascular Biology of the Placenta [Internet]. San Rafael: Morgan & Claypool Life Science Publishers; 2010 [cited November 10th 2018]. Available from PubMed: https://www.ncbi.nlm.nih.gov/books/NBK53245/.
76. Bernhard W, Viron A. Improved techniques for the preparation of ultrathin frozen sections. J Cell Biol. 1971;49(3):731-46.
77. Nystad M, Sitras V, Larsen M, Acharya G. Placental expression of aminopeptidase-Q (laeverin) and its role in the pathophysiology of preeclampsia. Am J Obstet Gynecol. 2014;211(6):686 e1-31.
78. Kovats S, Main EK, Librach C, Stubblebine M, Fisher SJ, DeMars R. A class I antigen, HLA-G, expressed in human trophoblasts. Science. 1990;248(4952):220-3.
79. Tong M, Chamley LW. Placental extracellular vesicles and feto-maternal communication. Cold Spring Harb Perspect Med. 2015;5(3):a023028.
80. Alberts B, Johnson A, Lewis J, Morgan D, Raff M, Roberts K, *et al*. Energy Conversion: Mitochondria and Chloroplasts. Molecular Biology of The Cell. 6th ed. New York: Garland Science; 2015. p. 753-812.
81. Askelund KJ, Chamley LW. Trophoblast deportation part I: review of the evidence demonstrating trophoblast shedding and deportation during human pregnancy. Placenta. 2011;32(10):716-23.
82. Redman CW, Tannetta DS, Dragovic RA, Gardiner C, Southcombe JH, Collett GP, *et al*. Review: Does size matter? Placental debris and the pathophysiology of pre-eclampsia. Placenta. 2012;33 Suppl:S48-54.
83. Huppertz B. IFPA Award in Placentology Lecture: Biology of the placental syncytiotrophoblast--myths and facts. Placenta. 2010;31 Suppl:S75-81.
84. Roland CS, Hu J, Ren CE, Chen H, Li J, Varvoutis MS, *et al*. Morphological changes of placental syncytium and their implications for the pathogenesis of preeclampsia. Cell Mol Life Sci. 2016;73(2):365-76.
85. Heazell AE, Moll SJ, Jones CJ, Baker PN, Crocker IP. Formation of syncytial knots is increased by hyperoxia, hypoxia and reactive oxygen species. Placenta. 2007;28 Suppl A:S33-40.
86. Loukeris K, Sela R, Baergen RN. Syncytial knots as a reflection of placental maturity: reference values for 20 to 40 weeks' gestational age. Pediatr Dev Pathol. 2010;13(4):305-9.
87. Lunghi L, Ferretti ME, Medici S, Biondi C, Vesce F. Control of human trophoblast function. Reprod Biol Endocrinol. 2007;5:6.

88. Liu Z, Ren Z, Zhang J, Chuang CC, Kandaswamy E, Zhou T, *et al*. Role of ROS and Nutritional Antioxidants in Human Diseases. Front Physiol. 2018;9:477.
89. Wang Y, Walsh SW. Antioxidant activities and mRNA expression of superoxide dismutase, catalase, and glutathione peroxidase in normal and preeclamptic placentas. J Soc Gynecol Investig. 1996;3(4):179-84.
90. Walsh SW. Maternal-placental interactions of oxidative stress and antioxidants in preeclampsia. Semin Reprod Endocrinol. 1998;16(1):93-104.

Appendix

Appendix A: Consent form

A consent form was given to the pregnant women in Norwegian to ensure that they understood what they consented to. This form is translated and contains the same information that was given to the women.

Preeclampsia is a disease affecting pregnant women with an incidence of 8-10 % worldwide and 4 % in Norway. The disease is potentially life-threatening disease for both the mother and her unborn child. Women with the condition have high blood pressure, proteins in their urine, edemas in the body and may affect different organs. The placenta has an important role in the development of preeclampsia. The aim of this pilot study is to implement high-resolution microscopy of placental tissue as an analytic tool used in diagnostic and research.

I consent that information from conversations and examination during pregnancy, in addition to examination of placental tissue, can be registered and used for research.

The collected material can be used for necessary research with the purpose of finding new biological and medical knowledge regarding preeclampsia. I am aware that it takes a long time to find all important factors and therefore, there is no set end-date for this research project.

I confirm that sufficient information has been given regarding the use of data and what will be stored. I know that no data from this research can be linked to my name, that my participation is voluntary, and that my consent can be withdrawn at any point without specifying a reason. I am informed that this research requires approval from Datatilsynet and the Ethical committee, and that questions can be directed to the doctor, researcher or midwife that invited to participate in the study.

☐ Yes, I consent to research ……

(date, signature)

☐ No, I do not consent to research ……

(date, signature)

Appendix B: Raw data, total antioxidant capacity assay

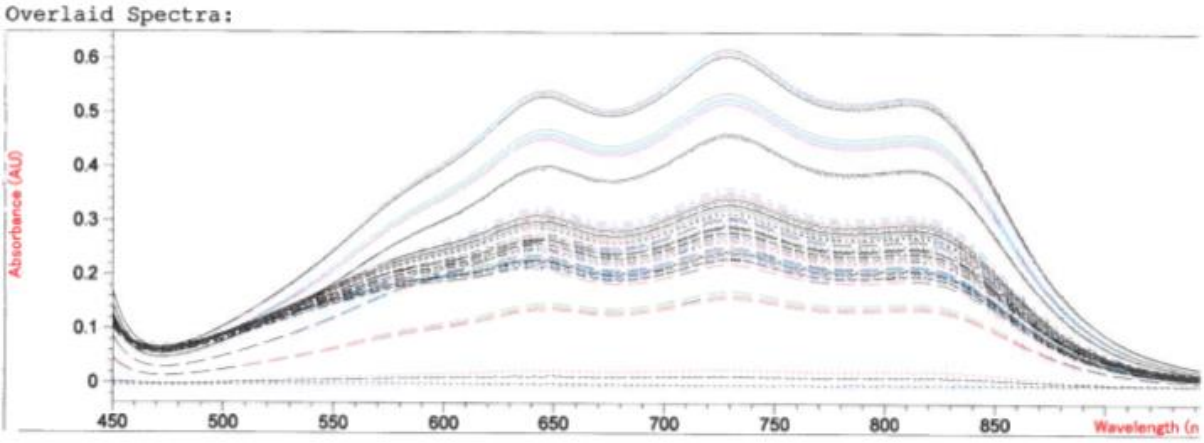

#	Name	Abs<730nm>	#	Name	Abs<730nm>
1	Vit C 0	0.60717	30	2P-F	0.33192
2	Vit C 0	0.61291	31	2P-M	0.30345
3	Vit C 0	0.61908	32	2P-M	0.27094
4	Vit C 1	0.52748	33	2P-M	0.27909
5	Vit C 1	0.51878	34	3P-F	0.31446
6	Vit C 1	0.53769	35	3P-F	0.29080
7	Vit C 2	0.45761	36	3P-F	0.29514
8	Vit C 2	0.46185	37	3P-M	0.26657
9	Vit C 2	0.46152	38	3P-M	0.24578
10	Vit C 4	0.30982	39	3P-M	0.26322
11	Vit C 4	0.30459	40	1N-F	0.32305
12	Vit C 4	0.30557	41	1N-F	0.33059
13	Vit C 6	0.15824	42	1N-F	0.33048
14	Vit C 6	0.17039	43	1N-M	0.28997
15	Vit C 6	0.16284	44	1N-M	0.28108
16	Vit C 8	1.3879E-2	45	1N-M	0.28783
17	Vit C 8	1.4417E-2	46	2N-F	0.25083
18	Vit C 8	2.6336E-2	47	2N-F	0.25002
19	Vit C 10	-2.5172E-3	48	2N-F	0.25396
20	Vit C 10	-3.2301E-3	49	2N-M	0.22071
21	Vit C 10	-2.1305E-3	50	2N-M	0.23843
22	1P-F	0.32695	51	2N-M	0.23233
23	1P-F	0.31905	52	3N-F	0.27886
24	1P-F	0.31412	53	3N-F	0.27354
25	1P-M	0.29078	54	3N-F	0.28473
26	1P-M	0.27816	55	3N-M	0.29954
27	1P-M	0.28004	56	3N-M	0.29194
28	2P-F	0.36071	57	3N-M	0.29193
29	2P-F	0.35352			

Appendix C: Raw data, oxidative stress assay

Table 23: Layout and raw data for the oxidative stress assay. *The first line in each square denotes the type of sample, whereas the second line is the measured optical density at 532 nm wavelength (OD_{532}) for the sample. Each sample was measured in two parallels.*

	1	2	3	4	5	6	7	8	9	10	11	12	
A													
B		0 nM 0.052	0 nM 0.054	4 nM 0.092	4 nM 0.099	8 nM 0.316	8 nM 0.321	12 nM 0.635	12 nM 0.642	16 nM 0.965	16 nM 0.972		OD_{532}
C		20 nM 1.358	20 nM 1.344										OD_{532}
D		1P-F 0.544	1P-F 0.562	1P-M 0.485	1P-M 0.472	2P-F 0.585	2P-F 0.591	2P-M 0.611	2P-M 0.621	3P-F 0.551	3P-F 0.552		OD_{532}
E		3P-M 0.395	3P-M 0.372										OD_{532}
F		1N-F 0.377	1N-F 0.365	1N-M 0.387	1N-M 0.395	2N-F 0.412	2N-F 0.425	2N-M 0.414	2N-M 0.423	3N-F 0.545	3N-F 0.536		OD_{532}
G		3N-M 0.454	3N-M 0.444										OD_{532}
H													